Fundamentals of Photonics
Bahaa E. A. Saleh, Malvin Carl Teich

ISBNs: 0-471-83965-5 (Hardback); 0-471-2-1374-8 (Electronic)

CHAPTER
16

SEMICONDUCTOR PHOTON SOURCES



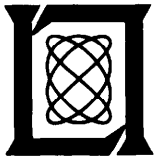

The operation of semiconductor injection lasers was reported nearly simultaneously in 1962 by independent research teams from **General Electric** Corporation, **IBM** Corporation, and **Lincoln Laboratory** of the Massachusetts Institute of Technology.

Light can be emitted from a semiconductor material as a result of electron–hole recombination. However, materials capable of emitting such light do not glow at room temperature because the concentrations of thermally excited electrons and holes are too low to produce discernible radiation. On the other hand, an external source of energy can be used to excite electron–hole pairs in sufficient numbers such that they produce large amounts of spontaneous recombination radiation, causing the material to glow or luminesce. A convenient way of achieving this is to forward bias a p–n junction, which has the effect of injecting electrons and holes into the same region of space; the resulting recombination radiation is then called **injection electroluminescence.**

A light-emitting diode (LED) is a forward-biased p–n junction fabricated from a direct-gap semiconductor material that emits light via injection electroluminescence [Fig. 16.0-1(a)]. If the forward voltage is increased beyond a certain value, the number of electrons and holes in the junction region can become sufficiently large so that a population inversion is achieved, whereupon stimulated emission (viz., emission induced by the presence of photons) becomes more prevalent than absorption. The junction may then be used as a diode laser amplifier [Fig. 16.0-1(b)] or, with appropriate feedback, as an injection laser diode [Fig. 16.0-1(c)].

Semiconductor photon sources, in the form of both LEDs and injection lasers, serve as highly efficient electronic-to-photonic transducers. They are convenient because they are readily modulated by controlling the injected current. Their small size, high efficiency, high reliability, and compatibility with electronic systems are important factors in their successful use in many applications. These include lamp indicators;

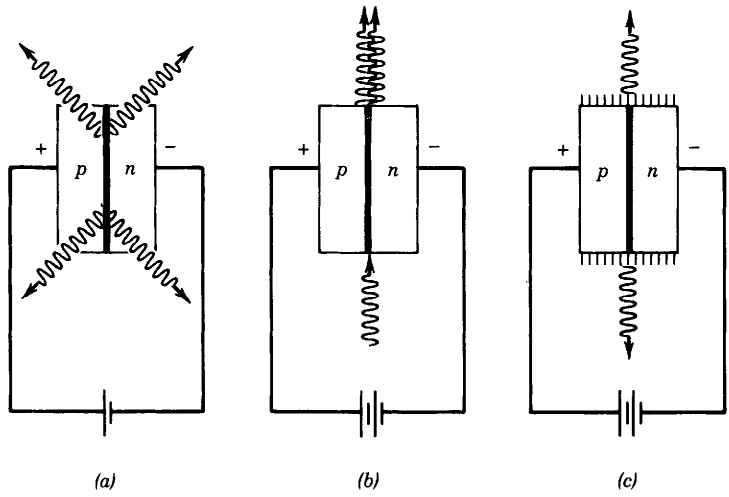

Figure 16.0-1 A forward-biased semiconductor p–n junction diode operated as (a) an LED, (b) a semiconductor optical amplifier, and (c) a semiconductor injection laser.

display devices; scanning, reading, and printing systems; fiber-optic communication systems; and optical data storage systems such as compact-disc players.

This chapter is devoted to the study of the light-emitting diode (Sec. 16.1), the semiconductor laser amplifier (Sec. 16.2), and the semiconductor injection laser (Sec. 16.3). Our treatment draws on the material contained in Chap. 15. The analysis of semiconductor laser amplification and oscillation is closely related to that developed in Chaps. 13 and 14.

16.1 LIGHT-EMITTING DIODES

A. Injection Electroluminescence

Electroluminescence in Thermal Equilibrium

Electron–hole radiative recombination results in the emission of light from a semiconductor material. At room temperature the concentration of thermally excited electrons and holes is so small, however, that the generated photon flux is very small.

EXAMPLE 16.1-1. ***Photon Emission from GaAs in Thermal Equilibrium.*** At room temperature, the intrinsic concentration of electrons and holes in GaAs is $n_i \approx 1.8 \times 10^6$ cm^{-3} (see Table 15.1-4). Since the radiative electron–hole recombination parameter $\tau_r \approx 10^{-10}$ cm^3/s (as specified in Table 15.1-5 for certain conditions), the electroluminescence rate $\tau_r np = \tau_r n_i^2 \approx 324$ photons/cm^3-s, as discussed in Sec. 15.1D. Using the bandgap energy for GaAs, $E_g = 1.42$ eV $= 1.42 \times 1.6 \times 10^{-19}$ J, this emission rate corresponds to an optical power density $= 324 \times 1.42 \times 1.6 \times 10^{-19} \approx 7.4 \times 10^{-17}$ W/cm^3. A 2-μm layer of GaAs therefore produces an intensity $I \approx 1.5 \times 10^{-20}$ W/cm^2, which is negligible. Light emitted from a layer of GaAs thicker than about 2 μm suffers reabsorption.

If thermal equilibrium conditions are maintained, this intensity cannot be appreciably increased (or decreased) by doping the material. In accordance with the law of mass action provided in (15.1-12), the product np is fixed at n_i^2 if the material is not too heavily doped so that the recombination rate $\tau_r np = \tau_r n_i^2$ depends on the doping level only through τ_r. An abundance of electrons *and* holes is required for a large recombination rate; in an n-type semiconductor n is large but p is small, whereas the converse is true in a p-type semiconductor.

Electroluminescence in the Presence of Carrier Injection

The photon emission rate can be appreciably increased by using external means to produce excess electron–hole pairs in the material. This may be accomplished, for example, by illuminating the material with light, but it is typically achieved by forward biasing a p–n junction diode, which serves to inject carrier pairs into the junction region. This process is illustrated in Fig. 15.1-17 and will be explained further in Sec. 16.1B. The photon emission rate may be calculated from the electron–hole pair injection rate R (pairs/cm^3-s), where R plays the role of the laser pumping rate (see Sec. 13.2). The photon flux Φ (photons per second), generated within a volume V of

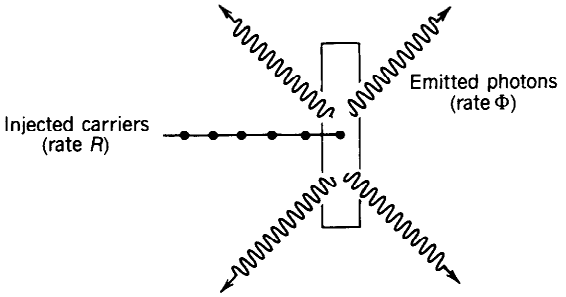

Figure 16.1-1 Spontaneous photon emission resulting from electron–hole radiative recombination, as might occur in a forward-biased p–n junction.

the semiconductor material, is directly proportional to the carrier-pair injection rate (see Fig. 16.1-1).

Denoting the equilibrium concentrations of electrons and holes in the absence of pumping as n_0 and p_0, respectively, we use $n = n_0 + \Delta n$ and $p = p_0 + \Delta p$ to represent the steady-state carrier concentrations in the presence of pumping (see Sec. 15.1D). The excess electron concentration Δn is precisely equal to the excess hole concentration Δp because electrons and holes are produced in pairs. It is assumed that the excess electron–hole pairs recombine at the rate $1/\tau$, where τ is the overall (radiative and nonradiative) electron–hole recombination time. Under steady-state conditions, the generation (pumping) rate must precisely balance the recombination (decay) rate, so that $R = \Delta n/\tau$. Thus the steady-state excess-carrier concentration is proportional to the pumping rate, i.e.,

$$\Delta n = R\tau. \tag{16.1-1}$$

For carrier injection rates that are sufficiently low, as explained in Sec. 15.1D, we have $\tau \approx 1/\mathscr{t}(n_0 + p_0)$, where $\mathscr{t}$ is the (radiative and nonradiative) recombination parameter, so that $R \approx \mathscr{t}\Delta n(n_0 + p_0)$.

Only radiative recombinations generate photons, however, and the internal quantum efficiency $\eta_i = \mathscr{t}_r/\mathscr{t} = \tau/\tau_r$, defined in (15.1-20) and (15.1-22), accounts for the fact that only a fraction of the recombinations are radiative in nature. The injection of RV carrier pairs per second therefore leads to the generation of a photon flux $\Phi = \eta_i RV$ photons/s, i.e.,

$$\boxed{\Phi = \eta_i RV = \eta_i \frac{V\Delta n}{\tau} = \frac{V\Delta n}{\tau_r}.} \tag{16.1-2}$$

The internal photon flux Φ is proportional to the carrier-pair injection rate R and therefore to the steady-state concentration of excess electron–hole pairs Δn.

The internal quantum efficiency η_i plays a crucial role in determining the performance of this electron-to-photon transducer. Direct-gap semiconductors are usually used to make LEDs (and injection lasers) because η_i is substantially larger than for

indirect-gap semiconductors (e.g., $\eta_i \approx 0.5$ for GaAs, whereas $\eta_i \approx 10^{-5}$ for Si, as shown in Table 15.1-5). The internal quantum efficiency η_i depends on the doping, temperature, and defect concentration of the material.

EXAMPLE 16.1-2. ***Injection Electroluminescence Emission from GaAs.*** Under certain conditions, $\tau = 50$ ns and $\eta_i = 0.5$ for GaAs (see Table 15.1-5), so that a steady-state excess concentration of injected electron–hole pairs $\Delta n = 10^{17}$ cm^{-3} will give rise to a photon flux concentration $\eta_i \Delta n/\tau \approx 10^{24}$ photons/cm^3-s. This corresponds to an optical power density $\approx 2.3 \times 10^5$ W/cm^3 for photons at the bandgap energy $E_g = 1.42$ eV. A 2-μm-thick slab of GaAs therefore produces an optical intensity of ≈ 46 W/cm^2, which is a factor of 10^{21} greater than the thermal equilibrium value calculated in Example 16.1-1. Under these conditions the power emitted from a device of area 200 μm $\times$ 10 μm is ≈ 0.9 mW.

Spectral Density of Electroluminescence Photons

The spectral density of injection electroluminescence light may be determined by using the direct band-to-band emission theory developed in Sec. 15.2. The rate of spontaneous emission $r_{sp}(\nu)$ (number of photons per second per hertz per unit volume), as provided in (15.2-16), is

$$r_{sp}(\nu) = \frac{1}{\tau_r} \varrho(\nu) f_e(\nu), \tag{16.1-3}$$

where τ_r is the radiative electron–hole recombination lifetime. The optical joint density of states for interaction with photons of frequency ν, as given in (15.2-9), is

$$\varrho(\nu) = \frac{(2m_r)^{3/2}}{\pi \hbar^2} (h\nu - E_g)^{1/2},$$

where m_r is related to the effective masses of the holes and electrons by $1/m_r = 1/m_v + 1/m_c$ [as given in (15.2-5)], and E_g is the bandgap energy. The emission condition [as given in (15.2-10)] provides

$$f_e(\nu) = f_c(E_2)[1 - f_v(E_1)], \tag{16.1-4}$$

which is the probability that a conduction-band state of energy

$$E_2 = E_c + \frac{m_r}{m_c}(h\nu - E_g) \tag{16.1-5}$$

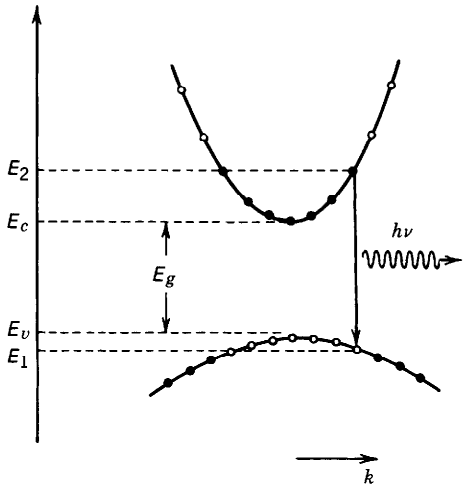

Figure 16.1-2 The spontaneous emission of a photon resulting from the recombination of an electron of energy E_2 with a hole of energy $E_1 = E_2 - h\nu$. The transition is represented by a vertical arrow because the momentum carried away by the photon, $h\nu/c$, is negligible on the scale of the figure.

is filled *and* a valence-band state of energy

$$E_1 = E_2 - h\nu \tag{16.1-6}$$

is empty, as provided in (15.2-6) and (15.2-7) and illustrated in Fig. 16.1-2. Equations (16.1-5) and (16.1-6) guarantee that energy and momentum are conserved. The Fermi functions $f_c(E) = 1/\{\exp[(E - E_{fc})/k_B T] + 1\}$ and $f_v(E) = 1/\{\exp[(E - E_{fv})/k_B T] + 1\}$ that appear in (16.1-4), with quasi-Fermi levels E_{fc} and E_{fv}, apply to the conduction and valence bands, respectively, under conditions of quasi-equilibrium.

The semiconductor parameters E_g, τ_r, m_v and m_c, and the temperature T determine the spectral distribution $r_{sp}(\nu)$, given the quasi-Fermi levels E_{fc} and E_{fv}. These, in turn, are determined from the concentrations of electrons and holes given in (15.1-7) and (15.1-8),

$$\int_{E_c}^{\infty} \varrho_c(E) f_c(E)\, dE = n = n_0 + \Delta n; \qquad \int_{-\infty}^{E_v} \varrho_v(E)[1 - f_v(E)]\, dE = p = p_0 + \Delta n. \tag{16.1-7}$$

The densities of states near the conduction- and valence-band edges are, respectively, as per (15.1-4) and (15.1-5),

$$\varrho_c(E) = \frac{(2m_c)^{3/2}}{2\pi^2\hbar^3}(E - E_c)^{1/2}; \qquad \varrho_v(E) = \frac{(2m_v)^{3/2}}{2\pi^2\hbar^3}(E_v - E)^{1/2},$$

where n_0 and p_0 are the concentrations of electrons and holes in thermal equilibrium (in the absence of injection), and $\Delta n = R\tau$ is the steady-state injected-carrier concentration. For sufficiently weak injection, such that the Fermi levels lie within the bandgap and away from the band edges by several $k_B T$, the Fermi functions may be approximated by their exponential tails. The spontaneous photon flux (integrated over

all frequencies) is then obtained from the spectral density $r_{sp}(\nu)$ by

$$\Phi = V\int_0^\infty r_{sp}(\nu)\,d\nu = \frac{V(m_r)^{3/2}}{\sqrt{2}\,\pi^{3/2}\hbar^3\tau_r}(k_BT)^{3/2}\exp\left(\frac{E_{fc}-E_{fv}-E_g}{k_BT}\right),$$

as is readily extrapolated from Problem 15.2-3.

Increasing the pumping level R causes Δn to increase, which, in turn, moves E_{fc} toward (or further into) the conduction band, and E_{fv} toward (or further into) the valence band. This results in an increase in the probability $f_c(E_2)$ of finding the conduction-band state of energy E_2 filled with an electron, and the probability $1 - f_v(E_1)$ of finding the valence-band state of energy E_1 empty (filled with a hole). The net result is that the emission-condition probability $f_e(\nu) = f_c(E_2)[1 - f_v(E_1)]$ increases with R, thereby enhancing the spontaneous emission rate given in (16.1-3) and the spontaneous photon flux Φ given above.

EXERCISE 16.1-1

Quasi-Fermi Levels of a Pumped Semiconductor

(a) Under ideal conditions at $T = 0$ K, when there is no thermal electron–hole pair generation [see Fig. 16.1-3(*a*)], show that the quasi-Fermi levels are related to the concentrations of injected electron–hole pairs Δn by

$$E_{fc} = E_c + (3\pi^2)^{2/3}\frac{\hbar^2}{2m_c}(\Delta n)^{2/3} \qquad (16.1\text{-}8a)$$

$$E_{fv} = E_v - (3\pi^2)^{2/3}\frac{\hbar^2}{2m_v}(\Delta n)^{2/3}, \qquad (16.1\text{-}8b)$$

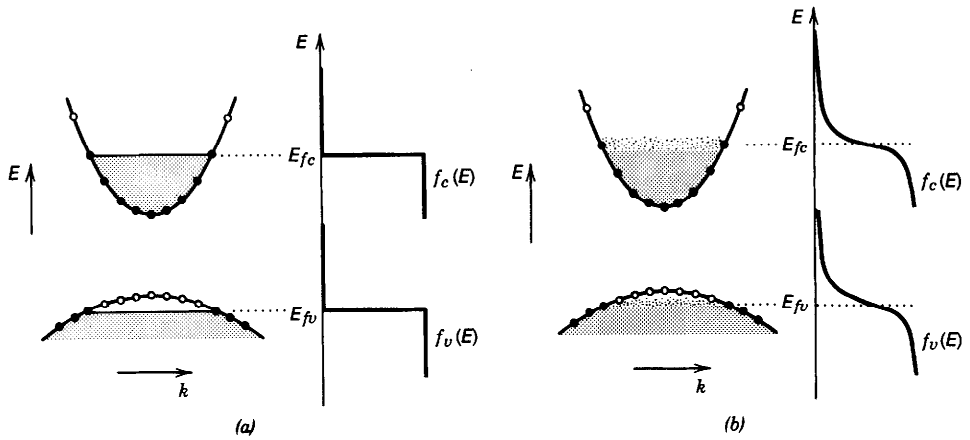

Figure 16.1-3 Energy bands and Fermi functions for a semiconductor in quasi-equilibrium (*a*) at $T = 0$ K, and (*b*) at $T > 0$ K.

so that

$$E_{fc} - E_{fv} = E_g + (3\pi^2)^{2/3} \frac{\hbar^2}{2m_r} (\Delta n)^{2/3}, \tag{16.1-8c}$$

where $\Delta n \gg n_0, p_0$. Under these conditions all Δn electrons occupy the lowest allowed energy levels in the conduction band, and all Δp holes occupy the highest allowed levels in the valence band. Compare with the results of Exercise 15.1-2.

(b) Sketch the functions $f_e(\nu)$ and $r_{sp}(\nu)$ for two values of Δn. Given the effect of temperature on the Fermi functions, as illustrated in Fig. 16.1-3(*b*), determine the effect of increasing the temperature on $r_{sp}(\nu)$.

EXERCISE 16.1-2

Spectral Density of Injection Electroluminescence Under Weak Injection. For sufficiently weak injection, such that $E_c - E_{fc} \gg k_B T$ and $E_{fv} - E_v \gg k_B T$, the Fermi functions may be approximated by their exponential tails. Show that the luminescence rate can then be expressed as

$$r_{sp}(\nu) = D(h\nu - E_g)^{1/2} \exp\left(-\frac{h\nu - E_g}{k_B T}\right), \qquad h\nu \geq E_g, \tag{16.1-9a}$$

where

$$D = \frac{(2m_r)^{3/2}}{\pi \hbar^2 \tau_r} \exp\left(\frac{E_{fc} - E_{fv} - E_g}{k_B T}\right) \tag{16.1-9b}$$

is an exponentially increasing function of the separation between the quasi-Fermi levels $E_{fc} - E_{fv}$. The spectral density of the spontaneous emission rate is shown in Fig. 16.1-4; it has precisely the same shape as the thermal-equilibrium spectral density shown in Fig. 15.2-9, but its magnitude is increased by the factor $D/D_0 = \exp[(E_{fc} - E_{fv})/k_B T]$, which can be very large in the presence of injection. In thermal equilibrium $E_{fc} = E_{fv}$, so that (15.2-20) and (15.2-21) are recovered.

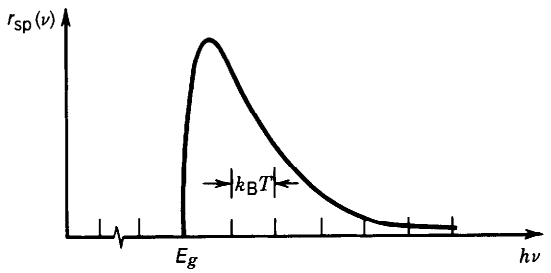

Figure 16.1-4 Spectral density of the direct band-to-band injection-electroluminescence rate $r_{sp}(\nu)$ (photons per second per hertz per cm^3), versus $h\nu$, from (16.1-9), under conditions of weak injection.

EXERCISE 16.1-3

Electroluminescence Spectral Linewidth

(a) Show that the spectral density of the emitted light described by (16.1-9) attains its peak value at a frequency ν_p determined by

$$h\nu_p = E_g + \frac{k_B T}{2}. \qquad (16.1\text{-}10)$$

Peak Frequency

(b) Show that the full width at half-maximum (FWHM) of the spectral density is

$$\Delta\nu \approx \frac{1.8 k_B T}{h}, \qquad (16.1\text{-}11)$$

Spectral Width (Hz)

(c) Show that this width corresponds to a wavelength spread $\Delta\lambda \approx 1.8\lambda_p^2 k_B T/hc$, where $\lambda_p = c/\nu_p$. For $k_B T$ expressed in eV and the wavelength expressed in μm, show that

$$\Delta\lambda \approx 1.45\lambda_p^2 k_B T. \qquad (16.1\text{-}12)$$

(d) Calculate $\Delta\nu$ and $\Delta\lambda$ at $T = 300$ K, for $\lambda_p = 0.8$ μm and $\lambda_p = 1.6$ μm.

B. LED Characteristics

As is clear from the foregoing discussion, the simultaneous availability of electrons and holes substantially enhances the flux of spontaneously emitted photons from a semiconductor. Electrons are abundant in n-type material, and holes are abundant in p-type material, but the generation of copious amounts of light requires that both electrons and holes be plentiful in the same region of space. This condition may be readily achieved in the junction region of a forward-biased p–n diode (see Sec. 15.1E). As shown in Fig. 16.1-5, forward biasing causes holes from the p side and electrons from the n side to be forced into the common junction region by the process of minority carrier injection, where they recombine and emit photons.

The light-emitting diode (LED) is a *forward-biased p–n junction* with a large radiative recombination rate arising from injected minority carriers. The semiconductor material is usually *direct-gap* to ensure high quantum efficiency. In this section we determine the output power, and spectral and spatial distributions of the light emitted from an LED and derive expressions for the efficiency, responsivity, and response time.

Internal Photon Flux

A schematic representation of a simple p–n junction diode is provided in Fig. 16.1-6. An injected dc current i leads to an increase in the steady-state carrier concentrations Δn, which, in turn, result in radiative recombination in the active-region volume V.

Since the total number of carriers per second passing through the junction region is i/e, where e is the magnitude of the electronic charge, the carrier injection (pumping)

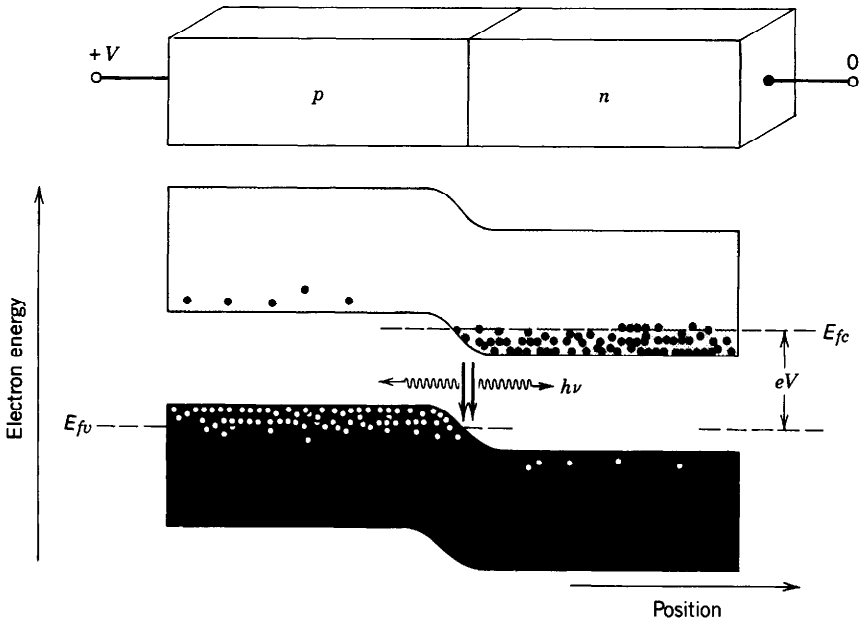

Figure 16.1-5 Energy diagram of a heavily doped p–n junction that is strongly forward biased by an applied voltage V. The dashed lines represent the quasi-Fermi levels, which are separated as a result of the bias. The simultaneous abundance of electrons and holes within the junction region results in strong electron–hole radiative recombination (injection electroluminescence).

rate (carriers per second per cm^3) is simply

$$R = \frac{i/e}{V}. \tag{16.1-13}$$

Equation (16.1-1) provides that $\Delta n = R\tau$, which results in a steady-state carrier concentration

$$\Delta n = \frac{(i/e)\tau}{V}. \tag{16.1-14}$$

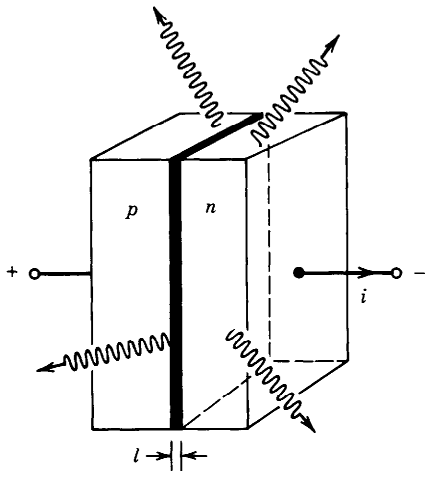

Figure 16.1-6 A simple forward-biased LED. The photons are emitted spontaneously from the junction region.

In accordance with (16.1-2), the generated photon flux Φ is then $\eta_i RV$, which, using (16.1-13), gives

$$\Phi = \eta_i \frac{i}{e}. \tag{16.1-15}$$

Internal Photon Flux

This simple and intuitively appealing formula governs the production of photons by electrons in an LED: a fraction η_i of the injected electron flux i/e (electrons per second) is converted into photon flux. The **internal quantum efficiency** η_i is therefore simply the ratio of the generated photon flux to the injected electron flux.

Output Photon Flux and Efficiency

The photon flux generated in the junction is radiated uniformly in all directions; however, the flux that emerges from the device depends on the direction of emission. This is readily illustrated by considering the photon flux transmitted through the material along three possible ray directions, denoted A, B, and C in the geometry of Fig. 16.1-7:

- The photon flux traveling in the direction of ray A is attenuated by the factor

$$\eta_1 = \exp(-\alpha l_1), \tag{16.1-16}$$

where α is the absorption coefficient of the n-type material and l_1 is the distance from the junction to the surface of the device. Furthermore, for normal incidence, reflection at the semiconductor–air boundary permits only a fraction of the light,

$$\eta_2 = 1 - \frac{(n-1)^2}{(n+1)^2} = \frac{4n}{(n+1)^2}, \tag{16.1-17}$$

to be transmitted, where n is the refractive index of the semiconductor material [see Fresnel's equations (6.2-14)]. For GaAs, $n = 3.6$, so that $\eta_2 = 0.68$. The overall transmittance for the photon flux traveling in the direction of ray A is therefore $\eta_A = \eta_1\eta_2$.

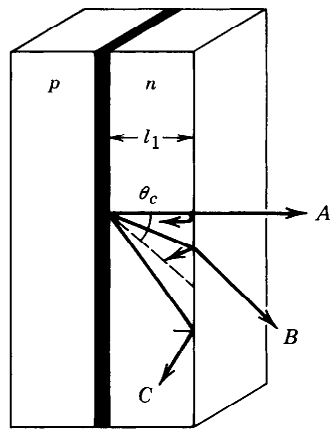

Figure 16.1-7 Not all light generated in an LED emerges from it. Ray A is partly reflected. Ray B suffers more reflection. Ray C lies outside the critical angle and therefore undergoes total internal reflection, so that, ideally, it cannot escape from the structure.

- The photon flux traveling in the direction of ray B has farther to travel and therefore suffers a larger absorption; it also has greater reflection losses. Thus $\eta_B < \eta_A$.
- The photon flux emitted along directions lying outside a cone of (critical) angle $\theta_c = \sin^{-1}(1/n)$, such as illustrated by ray C, suffer total internal reflection in an ideal material and are not transmitted at all [see (1.2-5)]. The fraction of emitted light lying within this cone is

$$\eta_3 = 1 - \cos\theta_c = 1 - \left(1 - \frac{1}{n^2}\right)^{1/2} \approx \frac{1}{2n^2}. \tag{16.1-18}$$

Thus, for $n = 3.6$, only 3.9% of the total generated photon flux can be transmitted. For a parallelepiped of refractive index $n > \sqrt{2}$, the ratio of isotropically generated light energy that can emerge, to the total generated light energy, is $3[1 - (1 - 1/n^2)^{1/2}]$, as shown in Exercise 1.2-6. However, in real LEDs, photons emitted outside the critical angle can be absorbed and re-emitted within this angle, so that in practice, η_3 may assume a value larger than that indicated in (16.1-18).

The output photon flux Φ_o is related to the internal photon flux by

$$\Phi_o = \eta_e \Phi = \eta_e \eta_i \frac{i}{e}, \tag{16.1-19}$$

where η_e is the overall transmission efficiency with which the internal photons can be extracted from the LED structure, and η_i relates the internal photon flux to the injected electron flux. A single quantum efficiency that accommodates both kinds of losses is the **external quantum efficiency** η_{ex},

$$\boxed{\eta_{ex} \equiv \eta_e \eta_i.} \tag{16.1-20}$$

External Quantum Efficiency

The output photon flux in (16.1-19) can therefore be written as

$$\boxed{\Phi_o = \eta_{ex} \frac{i}{e};} \tag{16.1-21}$$

External Photon Flux

η_{ex} is simply the ratio of the externally produced photon flux Φ_o to the injected electron flux. Because the pumping rate generally varies locally within the junction region, so does the generated photon flux.

The LED output optical power P_o is related to the output photon flux. Each photon has energy $h\nu$, so that

$$\boxed{P_o = h\nu\Phi_o = \eta_{ex} h\nu \frac{i}{e}.} \tag{16.1-22}$$

Output Power

Although η_i can be near unity for certain LEDs, η_{ex} generally falls well below unity, principally because of reabsorption of the light in the device and internal reflection at its boundaries. As a consequence, the external quantum efficiency of commonly encountered LEDs, such as those used in pocket calculators, is typically less than 1%.

Another measure of performance is the **overall quantum efficiency** η (also called the **power-conversion efficiency** or **wall-plug efficiency**), which is defined at the ratio of the emitted optical power P_o to the applied electrical power,

$$\eta \equiv \frac{P_o}{iV} = \eta_{ex}\frac{h\nu}{eV}, \tag{16.1-23}$$

where V is the voltage drop across the device. For $h\nu \approx eV$, as is the case for commonly encountered LEDs, it follows that $\eta \approx \eta_{ex}$.

Responsivity

The responsivity $\mathfrak{R}$ of an LED is defined as the ratio of the emitted optical power P_o to the injected current i, i.e., $\mathfrak{R} = P_o/i$. Using (16.1-22), we obtain

$$\mathfrak{R} = \frac{P_o}{i} = \frac{h\nu\Phi_o}{i} = \eta_{ex}\frac{h\nu}{e}. \tag{16.1-24}$$

The responsivity in W/A, when λ_o is expressed in μm, is then

$$\boxed{\mathfrak{R} = \eta_{ex}\frac{1.24}{\lambda_o}.} \tag{16.1-25}$$

LED Responsivity (W/A)
λ_o in μm

For example, if $\lambda_o = 1.24$ μm, then $\mathfrak{R} = \eta_{ex}$ W/A; if η_{ex} were unity, the maximum optical power that could be produced by an injection current of 1 mA would be 1 mW. However, as indicated above, typical values of η_{ex} for LEDs are in the range of 1 to 5%, so that LED responsivities are in the vicinity of 10 to 50 μW/mA.

In accordance with (16.1-22), the LED output power P_o should be proportional to the injected current i. In practice, however, this relationship is valid only over a restricted range. For the particular device whose light–current characteristic is shown in Fig. 16.1-8, the emitted optical power is proportional to the injection (drive) current only when the latter is less than about 75 mA. In this range, the responsivity has a

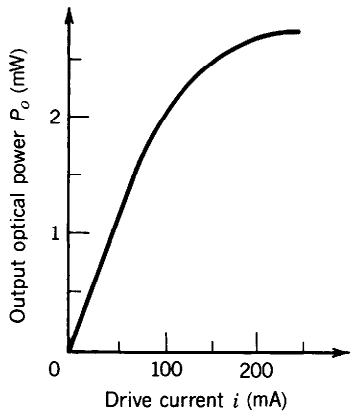

Figure 16.1-8 Optical power at the output of an actual LED versus injection (drive) current.

constant value of about 25 μW/mA, as determined from the slope of the curve. For larger drive currents, saturation causes the proportionality to fail; the responsivity is then no longer constant but rather declines with increasing drive current.

Spectral Distribution

The spectral density $r_{sp}(\nu)$ of light spontaneously emitted from a semiconductor in quasi-equilibrium has been determined, as a function of the concentration of injected carriers Δn, in Exercises 16.1-2 and 16.1-3. This theory is applicable to the electroluminescence light emitted from an LED in which quasi-equilibrium conditions are established by injecting current into a p–n junction.

Under conditions of weak pumping, such that the quasi-Fermi levels lie within the bandgap and are at least a few $k_B T$ away from the band edges, the spectral density achieves its peak value at the frequency $\nu_p = (E_g + k_B T/2)/h$ (see Exercise 16.1-3). In accordance with (16.1-11) and (16.1-12), the FWHM of the spectral density is $\Delta\nu \approx 1.8 k_B T/h$ ($\Delta\nu = 10$ THz for $T = 300$ K), which is independent of ν. The width expressed in terms of the wavelength does depend on λ,

$$\Delta\lambda \approx 1.45 \lambda_p^2 k_B T, \qquad (16.1\text{-}26)$$

Spectral Width (μm)

where $k_B T$ is expressed in eV, the wavelength is expressed in μm, and $\lambda_p = c/\nu_p$.

The proportionality of $\Delta\lambda$ to λ_p^2 is apparent in Fig. 16.1-9, which illustrates the observed wavelength spectral densities for a number of LEDs that operate in the visible and near-infrared regions. If $\lambda_p = 1$ μm at $T = 300$ K, for example, (16.1-26) provides $\Delta\lambda \approx 36$ nm.

Materials

LEDs have been operated from the near ultraviolet to the infrared, as illustrated in Fig. 16.1-9. In the near infrared, many binary semiconductor materials serve as highly efficient LED materials because of their direct-band gap nature. Examples of III–V

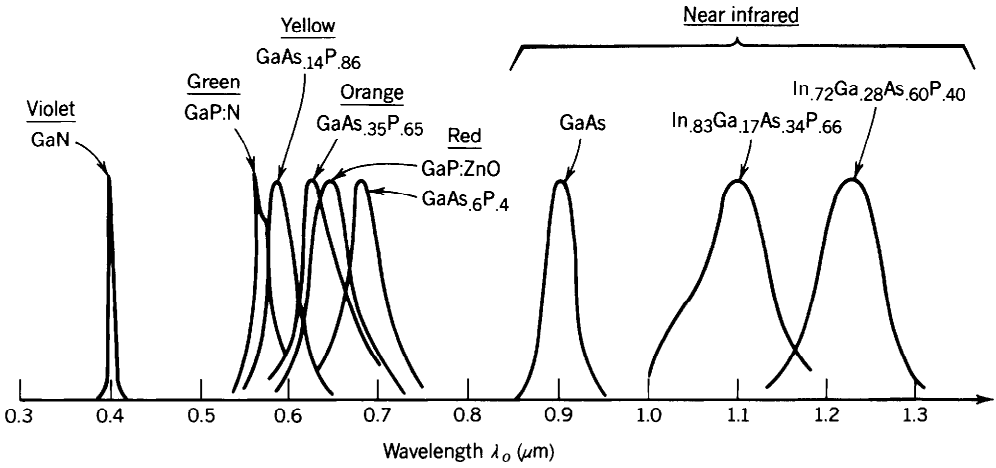

Figure 16.1-9 Spectral densities versus wavelength for semiconductor LEDs with different bandgaps. The peak intensities are normalized to the same value. The increasing spectral linewidth is a result of its proportionality to λ_p^2. (Adapted from S. M. Sze, *Physics of Semiconductor Devices*, Wiley, New York, 2nd ed. 1981.)

binary materials include (as shown in Table 15.1-3 and Fig. 15.1-5) GaAs ($\lambda_g = 0.87$ μm), GaSb (1.7 μm), InP (0.92 μm), InAs (3.5 μm), and InSb (7.3 μm). Ternary and quaternary compounds are also direct-gap over a wide range of compositions (see Fig. 15.1-5). These materials have the advantage that their emission wavelength can be compositionally tuned. Particularly important among the III–V compounds is ternary $Al_xGa_{1-x}As$ (0.75 to 0.87 μm) and quaternary $In_{1-x}Ga_xAs_{1-y}P_y$ (1.1 to 1.6 μm).

At short wavelengths (in the ultraviolet and most of the visible spectrum) materials such as GaN, GaP, and $GaAs_{1-x}P_x$ are typically used despite their low internal quantum efficiencies. These materials are often doped with elements that serve to enhance radiative recombination by acting as recombination centers. LEDs that emit blue light can also be made by using a phosphor to up-convert near-infrared photons from a GaAs LED (see Fig. 12.4-2).

Response Time

The response time of an LED is limited principally by the lifetime τ of the injected minority carriers that are responsible for radiative recombination. For a sufficiently small injection rate R, the injection/recombination process can be described by a first-order linear differential equation (see Sec. 15.1D), and therefore by the response to sinusoidal signals. An experimental determination of the highest frequency at which an LED can be effectively modulated is easily obtained by measuring the output light power in response to sinusoidal electric currents of different frequencies. If the injected current assumes the form $i = i_0 + i_1 \cos(\Omega t)$, where i_1 is sufficiently small so that the emitted optical power P varies linearly with the injected current, the emitted optical power behaves as $P = P_0 + P_1 \cos(\Omega t + \varphi)$.

The associated transfer function, which is defined as $\mathcal{H}(\Omega) = (P_1/i_1)\exp(j\varphi)$, assumes the form

$$\mathcal{H}(\Omega) = \frac{\Re}{1 + j\Omega\tau}, \tag{16.1-27}$$

which is characteristic of a resistor–capacitor circuit. The rise time of the LED is τ (seconds) and its 3-dB bandwidth is $B = 1/2\pi\tau$ (Hz). A larger bandwidth B is therefore attained by decreasing the rise time τ, which comprises contributions from both the radiative lifetime τ_r and the nonradiative lifetime τ_{nr} through the relation $1/\tau = 1/\tau_r + 1/\tau_{nr}$. However, reducing τ_{nr} results in an undesirable reduction of the internal quantum efficiency $\eta_i = \tau/\tau_r$. It may therefore be desirable to maximize the internal quantum efficiency–bandwidth product $\eta_i B = 1/2\pi\tau_r$ rather than maximizing the bandwidth alone. This requires a reduction of only the radiative lifetime τ_r, without a reduction of τ_{nr}, which may be achieved by careful choice of semiconductor material and doping level. Typical rise times of LEDs fall in the range 1 to 50 ns, corresponding to bandwidths as large as hundreds of MHz.

Device Structures

LEDs may be constructed either in surface-emitting or edge-emitting configurations (Fig. 16.1-10). The surface-emitting LED emits light from a face of the device that is parallel to the junction plane. Light emitted from the opposite face is absorbed by the substrate and lost or, preferably, reflected from a metallic contact (which is possible if a transparent substrate is used). The edge-emitting LED emits light from the edge of the junction region. The latter structure has usually been used for diode lasers as well, although surface-emitting laser diodes (SELDs) are being increasingly used. Surface-emitting LEDs are generally more efficient than edge-emitting LEDs. Heterostructure LEDs, with configurations such as those described in Sec. 16.2C, provide superior performance.

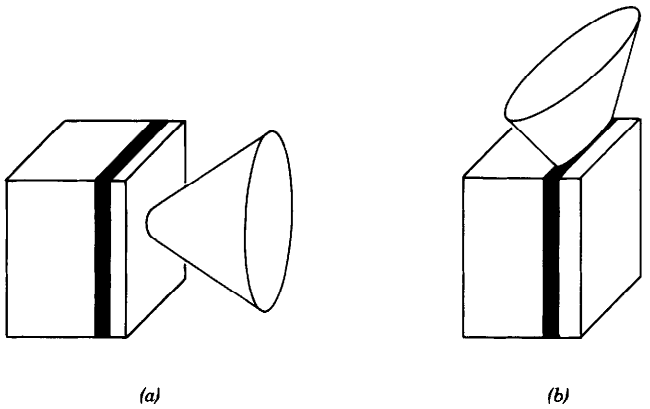

Figure 16.1-10 (a) Surface-emitting LED. (b) Edge-emitting LED.

Examples of surface-emitting LED structures are illustrated in Fig. 16.1-11. A flat-diode-configuration $GaAs_{1-x}P_x$ LED on a GaAs substrate is shown in Fig. 16.1-11(a). A layer of graded $GaAs_{1-y}P_y$, placed between the substrate and the n-type layer, reduces the lattice mismatch. The bandgap of GaAs is smaller than the photon energy of the emitted red light so that the radiation emitted toward the substrate is absorbed. Alternatively, transparent substrates such as GaP can be used in conjunction with a reflective contact to increase the external quantum efficiency. The Burrus-type LED, shown in Fig. 16.1-11(b), makes use of an etched well to permit the light to be collected directly from the junction region. This structure is particularly suitable for efficient coupling of the emitted light into an optical fiber, which may be brought into close proximity with the active region (see Fig. 22.1-5).

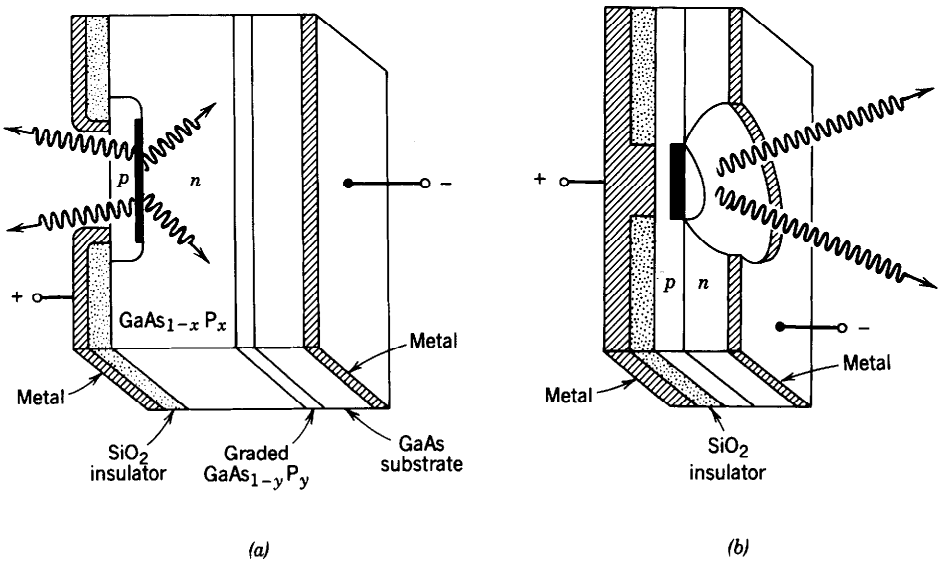

Figure 16.1-11 (a) A flat-diode-configuration $GaAs_{1-x}P_x$ LED. (b) A Burrus-type LED.

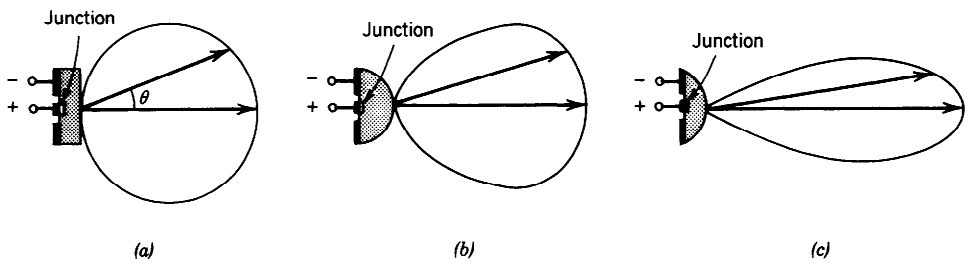

Figure 16.1-12 Radiation patterns of surface-emitting LEDs: (*a*) Lambertian pattern of a surface-emitting LED in the absence of a lens; (*b*) pattern of an LED with a hemispherical lens; (*c*) pattern of an LED with a parabolic lens.

Spatial Pattern of Emitted Light

The far-field radiation pattern from a surface-emitting LED is similar to that from a Lambertian radiator; the intensity varies as $\cos\theta$, where θ is the angle from the emission-plane normal. The intensity decreases to half its value at $\theta = 60°$. Epoxy lenses are often placed on the LED to reduce this angular spread. Differently shaped lenses alter the angular dependence of the emission pattern in specified ways as shown schematically in Fig. 16.1-12.

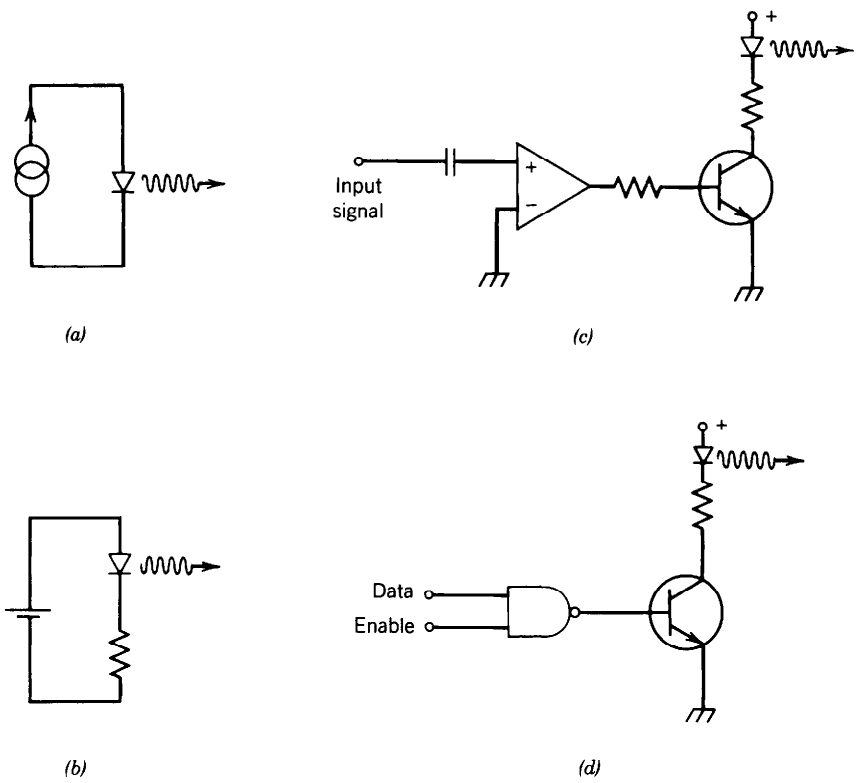

Figure 16.1-13 Various circuits can be used to drive an LED. These include (*a*) an ideal dc current source; (*b*) a dc current source provided by a constant-voltage source in series with a resistor; (*c*) transistor control of the current injected into the LED to provide analog modulation of the emitted light; (*d*) transistor switching of the current injected into the LED to provide digital modulation of the emitted light.

The radiation emitted from edge-emitting LEDs (and laser diodes) usually has a narrower radiation pattern. This pattern can often be well modeled by the function $\cos^s(\theta)$, where $s > 1$. If $s = 10$, for example, the intensity drops to half its value at $\theta \approx 21°$.

Electronic Circuitry

An LED is usually driven by a current source, as shown schematically in Fig. 16.1-13(*a*), for example by use of a constant-voltage source in series with a resistor, as illustrated in Fig. 16.1-13(*b*). The emitted light may be readily modulated (in either analog or digital format) simply by modulating the injected current. Two examples of such circuitry are the analog circuit shown in Fig. 16.1-13(*c*) and the digital circuit shown in Fig. 16.1-13(*d*). The performance of these circuits may be improved by adding bias current regulators, impedance matching circuitry, and nonlinear compensation circuitry. Furthermore, fluctuations in the intensity of the emitted light may be stabilized by the use of optical feedback in which the emitted light is monitored and used to control the injected current.

16.2 SEMICONDUCTOR LASER AMPLIFIERS

The principle underlying the operation of a semiconductor laser amplifier is the same as that for other laser amplifiers: the creation of a population inversion that renders stimulated emission more prevalent than absorption. The population inversion is usually achieved by electric current injection in a p–n junction diode; a forward bias voltage causes carrier pairs to be injected into the junction region, where they recombine by means of stimulated emission.

The theory of the semiconductor laser amplifier is somewhat more complex than that presented in Chap. 13 for other laser amplifiers, inasmuch as the transitions take place between bands of closely spaced energy levels rather than well-separated discrete levels. For purposes of comparison, nevertheless, the semiconductor laser amplifier may be viewed as a four-level laser system (see Fig. 13.2-6) in which the upper two levels lie in the conduction band and the lower two levels lie in the valence band.

The extension of the laser amplifier theory given in Chap. 13 to semiconductor structures has been provided in Chap. 15. In this section we use the results derived in Sec. 15.2 to obtain expressions for the gain and bandwidth of semiconductor laser amplifiers. We also review pumping schemes used for attaining a population inversion and briefly discuss semiconductor amplifier structures of current interest. The theoretical underpinnings of semiconductor laser amplifiers form the basis of injection laser operation, considered in Sec. 16.3.

Most semiconductor laser amplifiers fabricated to date are designed to operate in 1.3- to 1.55-μm lightwave communication systems as nonregenerative repeaters, optical preamplifiers, or narrowband electrically tunable amplifiers. In comparison with Er^{3+}:silica fiber amplifiers, semiconductor amplifiers have both advantages and disadvantages. They are smaller in size and are readily incorporated into optoelectronic integrated circuits. Their bandwidths can be as large as 10 THz, which is greater than that of fiber amplifiers. On the negative side, semiconductor amplifiers currently have greater insertion losses (typically 3 to 5 dB per facet) than fiber amplifiers. Furthermore, temperature instability, as well as polarization sensitivity, are difficult to overcome.

If a semiconductor laser amplifier is to be operated as a broadband single-pass device (i.e., as a traveling-wave amplifier), care must be taken to reduce the facet reflectances to very low values. Failure to do so would result in multiple reflections and

a gain profile modulated by the resonator modes; this could also lead to oscillation, which, of course, obviates the possibility of controllable amplification. The response time is determined by complex carrier dynamics; the shortest value to date is $\approx$ 100 ps.

A. Gain

Light of frequency ν can interact with the carriers of a semiconductor material of bandgap energy E_g via band-to-band transitions, provided that $\nu > E_g/h$. The incident photons may be absorbed resulting in the generation of electron–hole pairs, or they may produce additional photons through stimulated electron–hole recombination radiation (see Fig. 16.2-1). When emission is more likely than absorption, net optical gain ensues and the material can serve as a coherent optical amplifier.

Expressions for the rate of photon absorption $r_{ab}(\nu)$ and the rate of stimulated emission $r_{st}(\nu)$ were provided in (15.2-18) and (15.2-17). These quantities depend on the photon-flux spectral density ϕ_ν, the quantum-mechanical strength of the transition for the particular material under consideration (which is implicit in the value of the electron–hole radiative recombination lifetime τ_r), the optical joint density of states $\varrho(\nu)$, and the occupancy probabilities for emission and absorption, $f_e(\nu)$ and $f_a(\nu)$.

The optical joint density of states $\varrho(\nu)$ is determined by the E–k relations for electrons and holes and by the conservation of energy and momentum. With the help of the parabolic approximation for the E–k relations near the conduction- and valence-band edges, it was shown in (15.2-6) and (15.2-7) that the energies of the electron and hole that interact with a photon of energy $h\nu$ are

$$E_2 = E_c + \frac{m_r}{m_c}(h\nu - E_g), \qquad E_1 = E_2 - h\nu, \tag{16.2-1}$$

respectively, where m_c and m_v are their effective masses and $1/m_r = 1/m_c + 1/m_v$. The resulting optical joint density of states that interacts with a photon of energy $h\nu$ was determined to be [see (15.2-9)]

$$\varrho(\nu) = \frac{(2m_r)^{3/2}}{\pi\hbar^2}(h\nu - E_g)^{1/2}, \qquad h\nu \geq E_g. \tag{16.2-2}$$

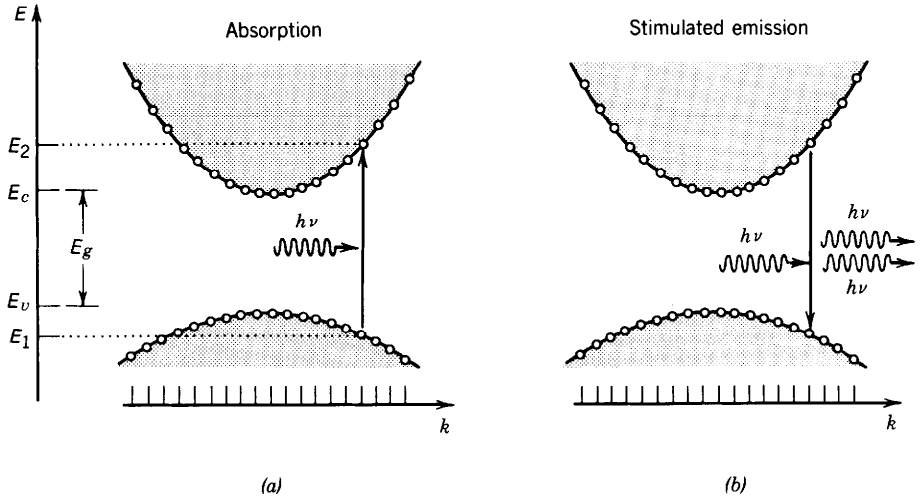

Figure 16.2-1 (*a*) The absorption of a photon results in the generation of an electron–hole pair. (*b*) Electron–hole recombination can be induced by a photon; the result is the stimulated emission of an identical photon.

It is apparent that $\varrho(\nu)$ increases as the square root of photon energy above the bandgap.

The occupancy probabilities $f_e(\nu)$ and $f_a(\nu)$ are determined by the pumping rate through the quasi-Fermi levels E_{fc} and E_{fv}. $f_e(\nu)$ is the probability that a conduction-band state of energy E_2 is filled with an electron and a valence-band state of energy E_1 is filled with a hole. $f_a(\nu)$, on the other hand, is the probability that a conduction-band state of energy E_2 is empty and a valence-band state of energy E_1 is filled with an electron. The Fermi inversion factor [see (15.2-24)]

$$f_g(\nu) = f_e(\nu) - f_a(\nu) = f_c(E_2) - f_v(E_1) \tag{16.2-3}$$

represents the degree of population inversion. $f_g(\nu)$ depends on both the Fermi function for the conduction band, $f_c(E) = 1/\{\exp[(E - E_{fc})/k_BT] + 1\}$, and the Fermi function for the valence band, $f_v(E) = 1/\{\exp[(E - E_{fv})/k_BT] + 1\}$. It is a function of temperature and of the quasi-Fermi levels E_{fc} and E_{fv}, which, in turn, are determined by the pumping rate. Because a complete population inversion can in principle be achieved in a semiconductor laser amplifier [$f_g(\nu) = 1$], it behaves like a four-level system.

The results provided above were combined in (15.2-23) to give an expression for the net gain coefficient, $\gamma_0(\nu) = [r_{st}(\nu) - r_{ab}(\nu)]/\phi_\nu$,

$$\gamma_0(\nu) = \frac{\lambda^2}{8\pi\tau_r}\varrho(\nu)f_g(\nu). \tag{16.2-4}$$

Gain Coefficient

Comparing (16.2-4) with (13.1-4), it is apparent that the quantity $\varrho(\nu)f_g(\nu)$ in the semiconductor laser amplifier plays the role of $Ng(\nu)$ in other laser amplifiers.

Amplifier Bandwidth

In accordance with (16.2-3) and (16.2-4), a semiconductor medium provides net optical gain at the frequency ν when $f_c(E_2) > f_v(E_1)$. Conversely, net attenuation ensues when $f_c(E_2) < f_v(E_1)$. Thus a semiconductor material in thermal equilibrium (undoped or doped) cannot provide net gain whatever its temperature; this is because the conduction- and valence-band Fermi levels coincide ($E_{fc} = E_{fv} = E_f$). External pumping is required to separate the Fermi levels of the two bands in order to achieve amplification.

The condition $f_c(E_2) > f_v(E_1)$ is equivalent to the requirement that the photon energy be smaller than the separation between the quasi-Fermi levels, i.e., $h\nu < E_{fc} - E_{fv}$, as demonstrated in Exercise 15.2-1. Of course, the photon energy must be larger than the bandgap energy ($h\nu > E_g$) in order that laser amplification occur by means of band-to-band transitions. Thus if the pumping rate is sufficiently large that the separation between the two quasi-Fermi levels exceeds the bandgap energy E_g, the medium can act as an amplifier for optical frequencies in the band

$$\frac{E_g}{h} < \nu < \frac{E_{fc} - E_{fv}}{h}. \tag{16.2-5}$$

Amplifier Bandwidth

For $h\nu < E_g$ the medium is transparent, whereas for $h\nu > E_{fc} - E_{fv}$ it is an attenuator instead of an amplifier. Equation (16.2-5) demonstrates that the amplifier bandwidth increases with $E_{fc} - E_{fv}$, and therefore with pumping level. In this respect it is unlike the atomic laser amplifier, which has an unsaturated bandwidth $\Delta\nu$ that is independent of pumping level (see Fig. 13.1-2).

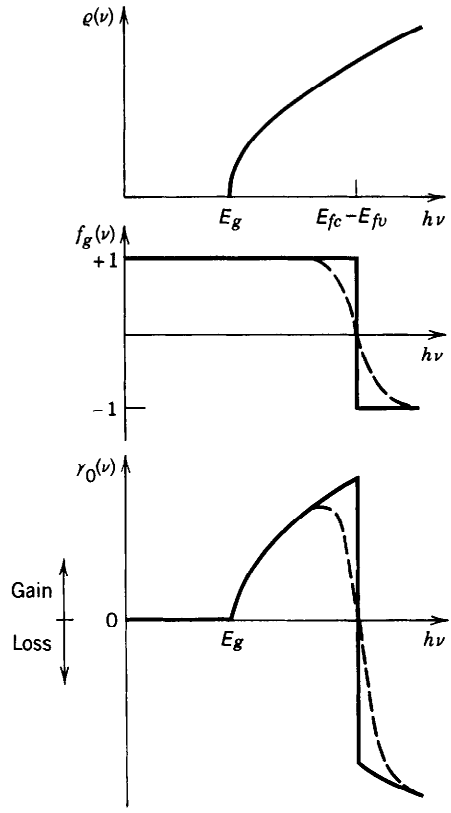

Figure 16.2-2 Dependence on energy of the joint optical density of states $\varrho(\nu)$, the Fermi inversion factor $f_g(\nu)$, and the gain coefficient $\gamma_0(\nu)$ at $T = 0$ K (solid curves) and at room temperature (dashed curves). Photons whose energy lies between E_g and $E_{fc} - E_{fv}$ undergo laser amplification.

Computation of the gain properties is simplified considerably if thermal excitations can be ignored (viz., $T = 0$ K). The Fermi functions are then simply $f_c(E_2) = 1$ for $E_2 < E_{fc}$ and 0 otherwise; $f_v(E_1) = 1$ for $E_1 < E_{fv}$ and 0 otherwise. In that case the Fermi inversion factor is

$$f_g(\nu) = \begin{cases} +1, & h\nu < E_{fc} - E_{fv} \\ -1, & \text{otherwise.} \end{cases} \tag{16.2-6}$$

Schematic plots of the functions $\varrho(\nu)$, $f_g(\nu)$, and the gain coefficient $\gamma_0(\nu)$ are presented in Fig. 16.2-2, illustrating how $\gamma_0(\nu)$ changes sign and turns into a loss coefficient when $h\nu > E_{fc} - E_{fv}$. The ν^{-2} dependence of $\gamma_0(\nu)$, arising from the λ^2 factor in the numerator of (16.2-4), is sufficiently slow that it may be ignored. Finite temperature smoothes the functions $f_g(\nu)$ and $\gamma_0(\nu)$, as shown by the dashed curves in Fig. 16.2-2.

Dependence of the Gain Coefficient on Pumping Level

The gain coefficient $\gamma_0(\nu)$ increases both in its width and in its magnitude as the pumping rate R is elevated. As provided in (16.1-1), a constant pumping rate R (number of injected excess electron–hole pairs per cm^3 per second) establishes a steady-state concentration of injected electron–hole pairs in accordance with $\Delta n = \Delta p = R\tau$, where τ is the electron–hole recombination lifetime (which includes both radiative and nonradiative contributions). Knowledge of the steady–steady total concentrations of electrons and holes, $n = n_0 + \Delta n$ and $p = p_0 + \Delta n$, respectively, permits the Fermi levels E_{fc} and E_{fv} to be determined via (16.1-7). Once the Fermi levels are known, the computation of the gain coefficient can proceed using (16.2-4). The

dependence of $\gamma_0(\nu)$ on Δn and thereby on R, is illustrated in Example 16.2-1. The onset of gain saturation and the noise performance of semiconductor laser amplifiers is similar to that of other amplifiers, as considered in Secs. 13.3 and 13.4.

EXAMPLE 16.2-1. ***InGaAsP Laser Amplifier.*** A room-temperature ($T = 300$ K) sample of $In_{0.72}Ga_{0.28}As_{0.6}P_{0.4}$ with $E_g = 0.95$ eV is operated as a semiconductor laser amplifier at $\lambda_o = 1.3$ μm. The sample is undoped but has residual concentrations of $\approx 2 \times 10^{17}$ cm^{-3} donors and acceptors, and a radiative electron–hole recombination lifetime $\tau_r \approx 2.5$ ns. The effective masses of the electrons and holes are $m_c \approx 0.06m_0$ and $m_v \approx 0.4m_0$, respectively, and the refractive index $n \approx 3.5$. Given the steady-state injected-carrier concentration Δn (which is controlled by the injection rate R and the overall recombination time τ), the gain coefficient $\gamma_0(\nu)$ may be computed from (16.2-4) in conjunction with (16.1-7). As illustrated in Fig. 16.2-3, both the amplifier bandwidth and the peak value of the gain coefficient γ_p increase with Δn. The energy at which the peak

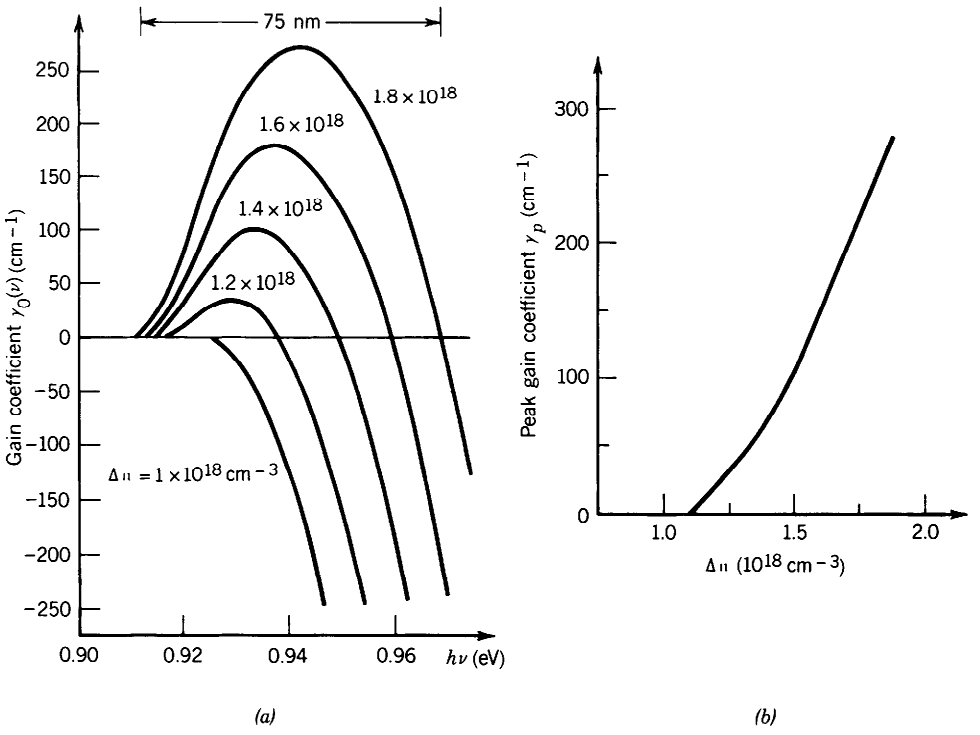

Figure 16.2-3 (*a*) Calculated gain coefficient $\gamma_0(\nu)$ for an InGaAsP laser amplifier versus photon energy $h\nu$, with the injected-carrier concentration Δn as a parameter ($T = 300$ K). The band of frequencies over which amplification occurs (centered near 1.3 μm) increases with increasing Δn. At the largest value of Δn shown, the full amplifier bandwidth is 15 THz, corresponding to 0.06 eV in energy, and 75 nm in wavelength. (Adapted from N. K. Dutta, Calculated Absorption, Emission, and Gain in $In_{0.72}Ga_{0.28}As_{0.6}P_{0.4}$, *Journal of Applied Physics*, vol. 51, pp. 6095–6100, 1980.) (*b*) Calculated peak gain coefficient γ_p as a function of Δn. At the largest value of Δn, the peak gain coefficient ≈ 270 cm^{-1}. (Adapted from N. K. Dutta and R. J. Nelson, The Case for Auger Recombination in $In_{1-x}Ga_xAs_yP_{1-y}$, *Journal of Applied Physics*, vol. 53, pp. 74–92, 1982.)

occurs also increases with Δn, as expected from the behavior shown in Fig. 16.2-2. Furthermore, the minimum energy at which amplification occurs decreases slightly with increasing Δn as a result of band-tail states, which reduce the bandgap energy. At the largest value of Δn shown ($\Delta n = 1.8 \times 10^{18}$ cm^{-3}), photons with energies falling between 0.91 and 0.97 eV undergo amplification. This corresponds to a full amplifier bandwidth of 15 THz, and a wavelength range of 75 nm, which is large in comparison with most atomic linewidths (see Table 13.2-1). The calculated peak gain coefficient $\gamma_p = 270$ cm^{-1} at this value of Δn is also large in comparison with most atomic laser amplifiers.

Approximate Peak Gain Coefficient

The complex dependence of the gain coefficient on the injected-carrier concentration makes the analysis of the semiconductor amplifier (and laser) somewhat difficult. Because of this, it is customary to adopt an empirical approach in which the peak gain coefficient γ_p is assumed to be linearly related to Δn for values of Δn near the operating point. As the example in Fig. 16.2-3(b) illustrates, this approximation is reasonable when γ_p is large. The dependence of the peak gain coefficient γ_p on Δn may then be modeled by the linear equation

$$\gamma_p \approx \alpha\left(\frac{\Delta n}{\Delta n_T} - 1\right), \tag{16.2-7}$$

Peak Gain Coefficient (Linear Approximation)

which is illustrated in Fig. 16.2-4. The parameters α and Δn_T are chosen to satisfy the following limits:

- When $\Delta n = 0$, $\gamma_p = -\alpha$, where α represents the absorption coefficient of the semiconductor in the absence of current injection.
- When $\Delta n = \Delta n_T$, $\gamma_p = 0$. Thus Δn_T is the injected-carrier concentration at which emission and absorption just balance so that the medium is transparent.

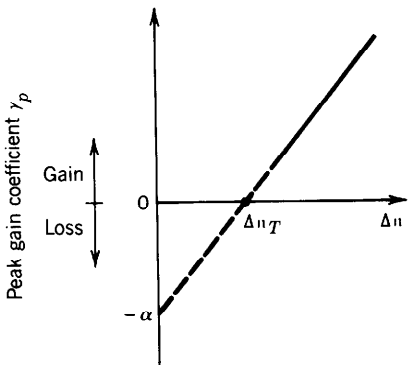

Figure 16.2-4 Peak value of the gain coefficient γ_p as a function of injected carrier concentration Δn for the approximate linear model. α represents the attenuation coefficient in the absence of injection, whereas Δn_T represents the injected carrier concentration at which emission and absorption just balance each other. The solid portion of the straight line matches the more realistic calculation considered in the preceding subsection.

EXAMPLE 16.2-2. ***InGaAsP Laser Amplifier.*** The peak gain coefficient γ_p versus Δn for InGaAsP presented in Fig. 16.2-3(b) may be approximately fit by a linear relation in the form of (16.2-7) with the parameters $\Delta n_T \approx 1.25 \times 10^{18}$ cm^{-3} and $\alpha = 600$ cm^{-1}. For $\Delta n = 1.4\,\Delta n_T = 1.75 \times 10^{18}$ cm^{-3}, the linear model yields a peak gain $\gamma_p = 240$ cm^{-1}. For an InGaAsP crystal of length $d = 350$ μm, this corresponds to a total gain of $\exp(\gamma_p d) \approx 4447$ or 36.5 dB. It must be kept in mind, however, that coupling losses are typically 3 to 5 dB per facet.

Increasing the injected-carrier concentration from below to above the transparency value Δn_T results in the semiconductor changing from a strong absorber of light [$f_g(\nu) < 0$] into a high-gain amplifier of light [$f_g(\nu) > 0$]. The very same large transition probability that makes the semiconductor a good absorber also makes it a good amplifier, as may be understood by comparing (15.2-17) and (15.2-18).

B. Pumping

Optical Pumping

Pumping may be achieved by the use of external light, as depicted in Fig. 16.2-5, provided that its photon energy is sufficiently large ($> E_g$). Pump photons are absorbed by the semiconductor, resulting in the generation of carrier pairs. The generated electrons and holes decay to the bottom of the conduction band and the top of the valence band, respectively. If the intraband relaxation time is much shorter than the interband relaxation time, as is usually the case, a steady-state population inversion between the bands may be established as discussed in Sec. 13.2.

Electric-Current Pumping

A more practical scheme for pumping a semiconductor is by means of electron–hole injection in a heavily doped p–n junction—a diode. As with the LED (see Sec. 16.1) the junction is forward biased so that minority carriers are injected into the junction region (electrons into the p-region and holes into the n-region). Figure 16.1-5 shows the energy-band diagram of a forward-biased heavily doped p–n junction. The conduction-band and valence-band quasi-Fermi levels E_{fc} and E_{fv} lie within the conduction and valence bands, respectively, and a state of quasi-equilibrium exists within the junction region. The quasi-Fermi levels are sufficiently well separated so that a population inversion is achieved and net gain may be obtained over the bandwidth

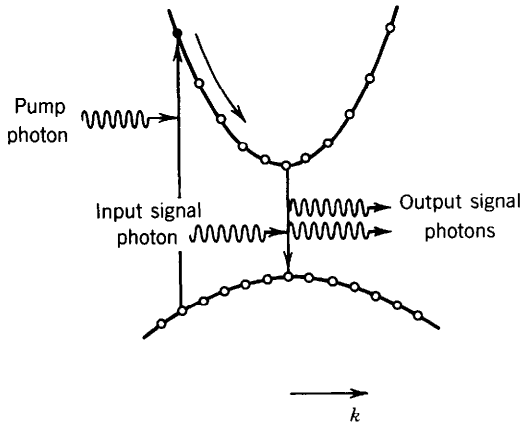

Figure 16.2-5 Optical pumping of a semiconductor laser amplifier.

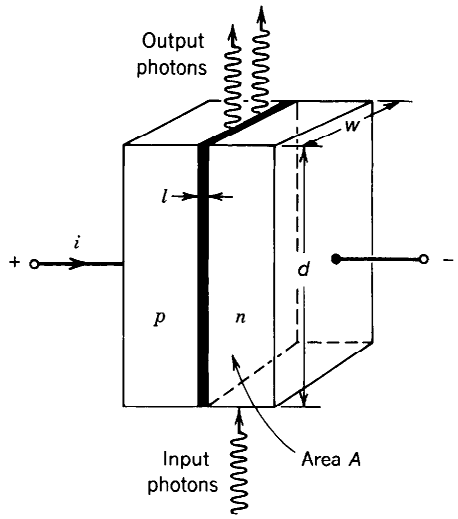

Figure 16.2-6 Geometry of a simple laser amplifier. Charge carriers travel perpendicularly to the p–n junction, whereas photons travel in the plane of the junction.

$E_g \leq h\nu \leq E_{fc} - E_{fv}$ within the active region. The thickness l of the active region is an important parameter of the diode that is determined principally by the diffusion lengths of the minority carriers at both sides of the junction. Typical values of l for InGaAsP are 1 to 3 μm.

If an electric current i is injected through an area $A = wd$, where w and d are the width and height of the device, respectively, into a volume lA (as shown in Fig. 16.2-6), then the steady-state carrier injection rate is $R = i/elA = J/el$ per second per unit volume, where $J = i/A$ is the injected current density. The resulting injected carrier concentration is then

$$\Delta n = \tau R = \frac{\tau}{elA} i = \frac{\tau}{el} J. \tag{16.2-8}$$

The injected carrier concentration is therefore directly proportional to the injected current density and the results shown in Figs. 16.2-3 and 16.2-4 with Δn as a parameter may just as well have J as a parameter. In particular, it follows from (16.2-7) and (16.2-8) that within the linear approximation implicit in (16.2-7), the peak gain coefficient is linearly related to the injected current density J, i.e.,

$$\boxed{\gamma_p \approx \alpha\left(\frac{J}{J_T} - 1\right).} \tag{16.2-9}$$

Peak Gain Coefficient

The transparency current density J_T is given by

$$\boxed{J_T = \frac{el}{\eta_i \tau_r} \Delta n_T}, \tag{16.2-10}$$

Transparency Current Density

where $\eta_i = \tau/\tau_r$ again represents the internal quantum efficiency.

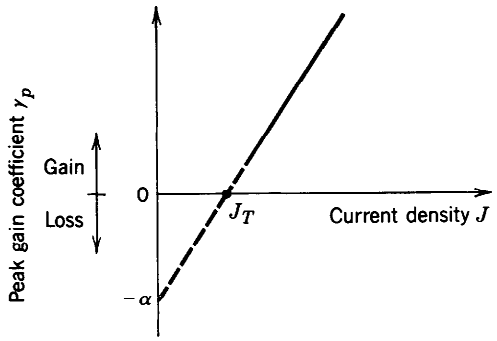

Figure 16.2-7 Peak optical gain coefficient γ_p as a function of current density J for the approximate linear model. When $J = J_T$ the material is transparent and exhibits neither gain nor loss.

When $J = 0$, the peak gain coefficient $\gamma_p = -\alpha$ becomes the attenuation coefficient, as is apparent in Fig. 16.2-7. When $J = J_T$, $\gamma_p = 0$ and the material is transparent and neither amplifies nor attenuates. Net gain can only be achieved when the injected current density J exceeds its transparency value J_T. Note that J_T is directly proportional to the junction thickness l so that a lower transparency current density J_T is achieved by using a narrower active-region thickness. This is an important consideration in the design of semiconductor amplifiers (and lasers).

EXAMPLE 16.2-3. ***InGaAsP Laser Amplifier.*** An InGaAsP diode laser amplifier operates at 300 K and has the following parameters: $\tau_r = 2.5$ ns, $\eta_i = 0.5$, $\Delta n_T = 1.25 \times 10^{18}$ cm^{-3}, and $\alpha = 600$ cm^{-1}. The junction has thickness $l = 2$ μm, length $d = 200$ μm, and width $w = 10$ μm. Using (16.2-10), the current density that just makes the semiconductor transparent is $J_T = 3.2 \times 10^4$ A/cm^2. A slightly larger current density $J = 3.5 \times 10^4$ A/cm^2 provides a peak gain coefficient $\gamma_p \approx 56$ cm^{-1} as is clear from (16.2-9). This gives rise to an amplifier gain $G = \exp(\gamma_p d) = \exp(1.12) \approx 3$. However, since the junction area $A = wd = 2 \times 10^{-5}$ cm^2, a rather large injection current $i = JA = 700$ mA is required to produce this current density.

Motivation for Heterostructures

If the thickness l of the active region in Example 16.2-3 were able to be reduced from 2 μm to, say, 0.1 μm, the current density J_T would be reduced by a factor of 20, to the more reasonable value 1600 A/cm^2. Because proportionately less volume would have to be pumped, the amplifier could then provide the same gain with a far lower injected current density. Reducing the thickness of the active region poses a problem, however, because the diffusion lengths of the electrons and holes in InGaAsP are several μm; the carriers would therefore tend to diffuse out of this smaller region. Is there a way in which these carriers can be confined to an active region whose thickness is smaller than their diffusion lengths? The answer is yes, by using a heterostructure device. These devices also make it possible to confine a light beam to an active region smaller than its wavelength, which provides further substantial advantage.

C. Heterostructures

As is apparent from (16.2-9) and (16.2-10), the diode-laser peak amplifier gain coefficient γ_p varies inversely with the thickness l of the active region. It is therefore advantageous to use the narrowest thickness possible. The active region is defined by the diffusion distances of minority carriers on both sides of the junction. The concept of the double heterostructure is to form heterojunction potential barriers on both sides of the p–n junction to provide a potential well that limits the distance over which minority carriers may diffuse. The junction barriers define a region of space within which minority carriers are confined, so that active regions of thickness l as small as 0.1 μm can be achieved. (Even thinner confinement regions, ≈ 0.01 μm, can be achieved with quantum-well lasers, as will be discussed in Sec. 16.3G.)

Electromagnetic confinement of the amplified optical beam can simultaneously be achieved if the material of the active layer is selected such that its refractive index is slightly greater than that of the two surrounding layers, so that the structure acts as an optical waveguide (see Chap. 7).

The double-heterostructure design therefore calls for three layers of different lattice-matched materials (see Fig. 16.2-8):

Layer 1: p-type, energy gap E_{g1}, refractive index n_1.
Layer 2: p-type, energy gap E_{g2}, refractive index n_2.
Layer 3: n-type, energy gap E_{g3}, refractive index n_3.

The materials are selected such that E_{g1} and E_{g3} are greater than E_{g2} to achieve carrier confinement, while n_2 is greater than n_1 and n_3 to achieve light confinement. The active layer (layer 2) is made quite thin (0.1 to 0.2 μm) to minimize the

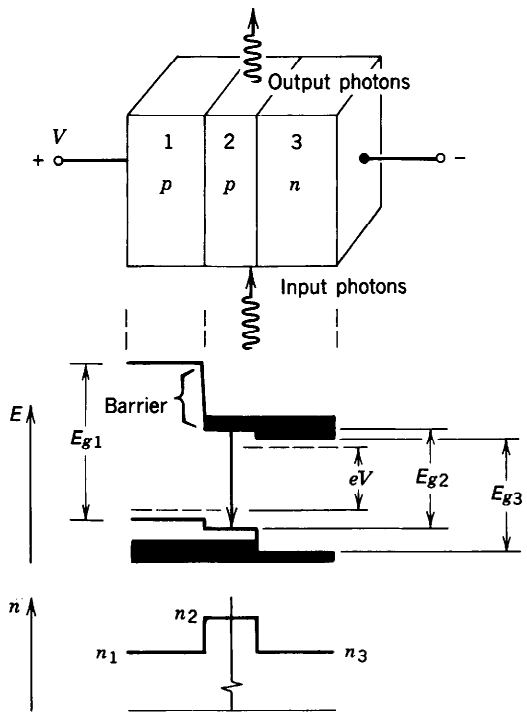

Figure 16.2-8 Energy-band diagram and refractive index as functions of position for a double-heterostructure semiconductor laser amplifier.

transparency current density J_T and maximize the peak gain coefficient γ_p. Stimulated emission takes place in the p–n junction region between layers 2 and 3.

In summary, the double-heterostructure design offers the following advantages:

- Increased amplifier gain, for a given injected current density, resulting from a decreased active-layer thickness [see (16.2-9) and (16.2-10)]. Injected minority carriers are confined within the thin active layer between the two heterojunction barriers and are prevented from diffusing to the surrounding layers.
- Increased amplifier gain resulting from the confinement of light within the active layer caused by its larger refractive index. The active medium acts as an optical waveguide.
- Reduced loss, resulting from the inability of layers 1 and 3 to absorb the guided photons because their bandgaps E_{g1} and E_{g3} are larger than the photon energy (i.e., $h\nu = E_{g2} < E_{g1}, E_{g2}$).

Two examples of double-heterostructure laser amplifiers are:

- *InGaAsP / InP Double-Heterostructure Laser Diode Amplifier.* The active layer is $In_{1-x}Ga_xAs_{1-y}P_y$, while the surrounding layers are InP. The ratios x and y are selected so that the materials are lattice matched. Operation is thereby restricted to a range of values of x and y for which E_{g2} corresponds to the band 1.1 to 1.7 μm.
- *GaAs / AlGaAs Double-Heterostructure Laser Diode Amplifier.* The active layer (layer 2) is fabricated from GaAs ($E_{g2} = 1.42$ eV, $n_2 = 3.6$). The surrounding layers (1 and 3) are fabricated from $Al_xGa_{1-x}As$ with $E_g > 1.43$ eV and $n < 3.6$ (by 5 to 10%). This amplifier typically operates within the 0.82- to 0.88-μm wavelength band using AlGaAs with $x = 0.35$ to 0.5.

16.3 SEMICONDUCTOR INJECTION LASERS

A. Amplification, Feedback, and Oscillation

A semiconductor injection laser is a semiconductor laser amplifier that is provided with a path for optical feedback. As discussed in the preceding section, a semiconductor laser amplifier is a forward-biased heavily doped p–n junction fabricated from a direct-gap semiconductor material. The injected current is sufficiently large to provide optical gain. The optical feedback is provided by mirrors, which are usually obtained by cleaving the semiconductor material along its crystal planes. The sharp refractive index difference between the crystal and the surrounding air causes the cleaved surfaces to act as reflectors. Thus the semiconductor crystal acts both as a gain medium and as an optical resonator, as illustrated in Fig. 16.3-1. Provided that the gain coefficient is sufficiently large, the feedback converts the optical amplifier into an optical oscillator (a laser). The device is called a semiconductor injection laser, or a laser diode.

The laser diode (LD) is similar to the light-emitting diode (LED) discussed in Sec. 16.1. In both devices, the source of energy is an electric current injected into a p–n junction. However, the light emitted from an LED is generated by spontaneous emission, whereas the light from an LD arises from stimulated emission.

In comparison with other types of lasers, injection lasers have a number of advantages: small size, high efficiency, integrability with electronic components, and ease of pumping and modulation by electric current injection. However, the spectral linewidth of semiconductor lasers is typically larger than that of other lasers.

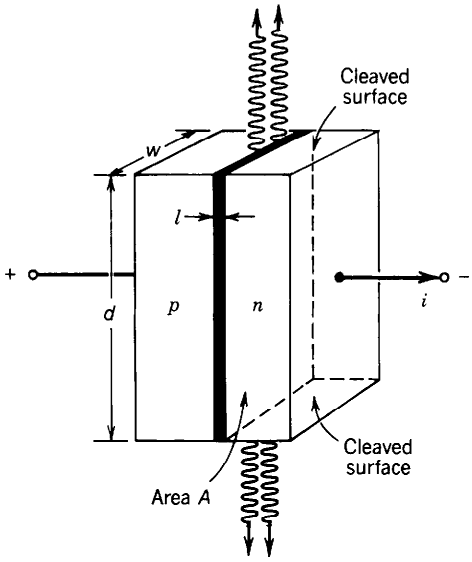

Figure 16.3-1 An injection laser is a forward-biased p–n junction with two parallel surfaces that act as reflectors.

We begin our study of the conditions required for laser oscillation, and the properties of the emitted light, with a brief summary of the basic results that describe the semiconductor laser amplifier and the optical resonator.

Laser Amplification

The gain coefficient $\gamma_0(\nu)$ of a semiconductor laser amplifier has a peak value γ_p that is approximately proportional to the injected carrier concentration, which, in turn, is proportional to the injected current density J. Thus, as provided in (16.2-9) and (16.2-10) and illustrated in Fig. 16.2-7,

$$\gamma_p \approx \alpha\left(\frac{J}{J_T} - 1\right), \qquad J_T = \frac{el}{\eta_i \tau_r}\Delta n_T, \tag{16.3-1}$$

where τ_r is the radiative electron–hole recombination lifetime, $\eta_i = \tau/\tau_r$ is the internal quantum efficiency, l is the thickness of the active region, α is the thermal-equilibrium absorption coefficient, and Δn_T and J_T are the injected-carrier concentration and current density required to just make the semiconductor transparent.

Feedback

The feedback is usually obtained by cleaving the crystal planes normal to the plane of the junction, or by polishing two parallel surfaces of the crystal. The active region of the p–n junction illustrated in Fig. 16.3-1 then also serves as a planar-mirror optical resonator of length d and cross-sectional area lw. Semiconductor materials typically have large refractive indices, so that the power reflectance at the semiconductor–air interface

$$\mathscr{R} = \left(\frac{n-1}{n+1}\right)^2 \tag{16.3-2}$$

is substantial (see (6.2-14) and Table 15.2-1). Thus if the gain of the medium is

sufficiently large, the refractive index discontinuity itself can serve as an adequate reflective surface and no external mirrors are necessary. For GaAs, for example, $n = 3.6$, so that (16.3-2) yields $\mathscr{R} = 0.32$.

Resonator Losses

The principal source of resonator loss arises from the partial reflection at the surfaces of the crystal. This loss constitutes the transmitted useful laser light. For a resonator of length d the reflection loss coefficient is [see (9.1-18)]

$$\alpha_m = \alpha_{m1} + \alpha_{m2} = \frac{1}{2d} \ln \frac{1}{\mathscr{R}_1 \mathscr{R}_2}; \tag{16.3-3}$$

if the two surfaces have the same reflectance $\mathscr{R}_1 = \mathscr{R}_2 = \mathscr{R}$, then $\alpha_m = (1/d)\ln(1/\mathscr{R})$. The total loss coefficient is

$$\alpha_r = \alpha_s + \alpha_m, \tag{16.3-4}$$

where α_s represents other sources of loss, including free carrier absorption in the semiconductor material (see Fig. 15.2-2) and scattering from optical inhomogeneities. α_s increases as the concentration of impurities and interfacial imperfections in heterostructures increase. It can attain values in the range 10 to 100 cm^{-1}.

Of course, the term $-\alpha$ in the expression for the gain coefficient (16.3-1), corresponding to absorption in the material, also contributes substantially to the losses. This contribution is accounted for, however, in the *net* peak gain coefficient γ_p given by (16.3-1). This is apparent from the expression for $\gamma_0(\nu)$ given in (15.2-23), which is proportional to $f_g(\nu) = f_e(\nu) - f_a(\nu)$ (i.e., to stimulated emission less absorption).

Another important contribution to the loss results from the spread of optical energy outside the active layer of the amplifier (in the direction *perpendicular* to the junction plane). This can be especially detrimental if the thickness of the active layer l is small. The light then propagates through a thin amplifying layer (the active region) surrounded by a lossy medium so that large losses are likely. This problem may be alleviated by the use of a double heterostructure (see Sec. 16.2C and Fig. 16.2-8), in which the middle layer is fabricated from a material of elevated refractive index that acts as a waveguide confining the optical energy.

Losses caused by optical spread may be phenomenologically accounted for by defining a **confinement factor** Γ to represent the fraction of the optical energy lying within the active region (Fig. 16.3-2). Assuming that the energy outside the active region is totally wasted, Γ is therefore the factor by which the gain coefficient is reduced, or equivalently, the factor by which the loss coefficient is increased. Equation (16.3-4) must therefore be modified to reflect this increase, so that

$$\alpha_r = \frac{1}{\Gamma}(\alpha_s + \alpha_m). \tag{16.3-5}$$

There are basically three types of laser-diode structures based on the mechanism used for confining the carriers or light in the lateral direction (viz., *in* the junction plane): **broad-area** (in which there is no mechanism for lateral confinement), **gain-guided** (in which lateral variations of the gain are used for confinement), and **index-guided** (in which lateral refractive index variations are used for confinement). Index-guided lasers are generally preferred because of their superior properties.

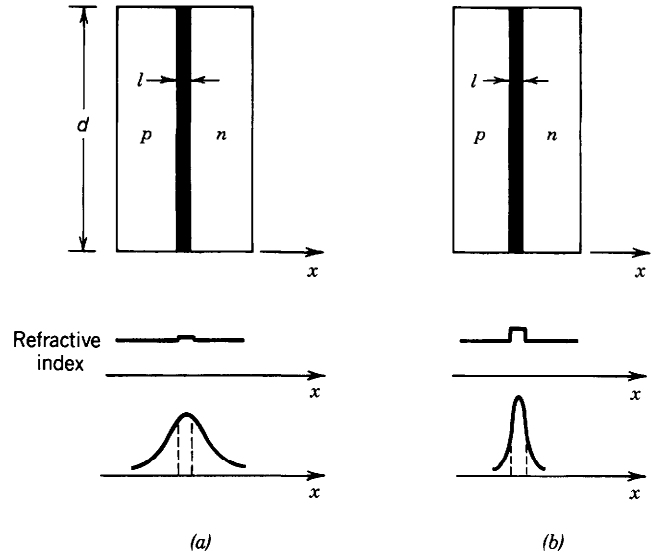

Figure 16.3-2 Spatial spread of the laser light in the direction perpendicular to the plane of the junction for (*a*) homostructure, and (*b*) heterostructure lasers.

Gain Condition: Laser Threshold

The laser oscillation condition is that the gain exceed the loss, $\gamma_p > \alpha_r$, as indicated in (14.1-10). The threshold gain coefficient is therefore α_r. Setting $\gamma_p = \alpha_r$ and $J = J_t$ in (16.3-1) corresponds to a threshold injected current density J_t given by

$$J_t = \frac{\alpha_r + \alpha}{\alpha} J_T, \tag{16.3-6}$$

Threshold Current Density

where the transparency current density,

$$J_T = \frac{el}{\eta_i \tau_r} \Delta n_T, \tag{16.3-7}$$

Transparency Current Density

is the current density that just makes the medium transparent. The threshold current density is larger than the transparency current density by the factor $(\alpha_r + \alpha)/\alpha$, which is ≈ 1 when $\alpha \gg \alpha_r$. Since the current $i = JA$, where $A = wd$ is the cross-sectional area of the active region, we can define $i_T = J_T A$ and $i_t = J_t A$, corresponding to the currents required to achieve transparency of the medium and laser oscillation threshold, respectively.

The threshold current density J_t is a key parameter in characterizing the diode-laser performance; smaller values of J_t indicate superior performance. In accordance with (16.3-6) and (16.3-7), J_t is minimized by maximizing the internal quantum efficiency η_i, and by minimizing the resonator loss coefficient α_r, the transparency injected-carrier concentration Δn_T, and the active-region thickness l. As l is reduced beyond a certain point, however, the loss coefficient α_r becomes larger because the confinement factor Γ decreases [see (16.3-5)]. Consequently, J_t decreases with decreasing l until it reaches

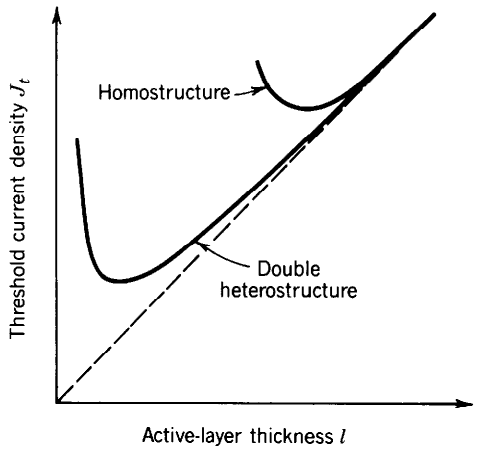

Figure 16.3-3 Dependence of the threshold current density J_t on the thickness of the active layer l. The double-heterostructure laser exhibits a lower value of J_t than the homostructure laser, and therefore superior performance.

a minimum value, beyond which any further reduction causes J_t to increase (see Fig. 16.3-3). In double-heterostructure lasers, however, the confinement factor remains near unity for lower values of l because the active layer behaves as an optical waveguide (see Fig. 16.3-2). The result is a lower minimum value of J_t, as shown in Fig. 16.3-3, and therefore superior performance. The reduction in J_t is illustrated in the following examples.

Because the parameters Δn_T and α in (16.3-1) strongly depend on temperature, so does the threshold current density J_t and the frequency at which the peak gain occurs. As a result, temperature control is required to stabilize the laser output. Indeed, frequency tuning is often achieved by deliberate modification of the temperature of operation.

EXAMPLE 16.3-1. ***Threshold Current for an InGaAsP Homostructure Laser Diode.*** Consider an InGaAsP homostructure semiconductor injection laser with the same material parameters as in Examples 16.2-1 and 16.2-2: $\Delta n_T = 1.25 \times 10^{18}$ cm^{-3}, $\alpha = 600$ cm^{-1}, $\tau_r = 2.5$ ns, $n = 3.5$, and $\eta_i = 0.5$ at $T = 300$ K. Assume that the dimensions of the junction are $d = 200$ μm, $w = 10$ μm, and $l = 2$ μm. The current density necessary for transparency is then calculated to be $J_T = 3.2 \times 10^4$ A/cm^2. We now determine the threshold current density for laser oscillation. Using (16.3-2), the surface reflectance is $\mathscr{R} = 0.31$. The corresponding mirror loss coefficient is $\alpha_m = (1/d)\ln(1/\mathscr{R}) = 59$ cm^{-1}. Assuming that the loss coefficient due to other effects is also $\alpha_s = 59$ cm^{-1} and that the confinement factor $\Gamma \approx 1$, the total loss coefficient is then $\alpha_r = 118$ cm^{-1}. The threshold current density is therefore $J_t = [(\alpha_r + \alpha)/\alpha]J_T = [(118 + 600)/600][3.2 \times 10^4] = 3.8 \times 10^4$ A/cm^2. The corresponding threshold current $i_t = J_t wd \approx 760$ mA, which is rather high. Homostructure lasers are no longer used because continuous-wave (CW) operation of devices with such large currents is not possible unless they are cooled substantially below $T = 300$ K to dissipate the heat.

EXAMPLE 16.3-2. ***Threshold Current for an InGaAsP Heterostructure Laser Diode.*** We turn now to an InGaAsP/InP double-heterostructure semiconductor injection laser (see Fig. 16.2-8) with the same parameters and dimensions as in Example 16.3-1 except for

the active-layer thickness, which is now $l = 0.1$ μm instead of 2 μm. If the confinement of light is assumed to be perfect ($\Gamma = 1$), we may use the same values for the resonator loss coefficient α_r. The transparency current density is then reduced by a factor of 20 to $J_T = 1600$ A/cm^2, and the threshold current density assumes a more reasonable value of $J_t = 1915$ A/cm^2. The corresponding threshold current is $i_t = 38$ mA. It is this significant reduction in threshold current that makes CW operation of the double-heterostructure laser diode at room temperature feasible.

B. Power

Internal Photon Flux

When the laser current density is increased above its threshold value (i.e., $J > J_t$), the amplifier peak gain coefficient γ_p exceeds the loss coefficient α_r. Stimulated emission then outweighs absorption and other resonator losses so that oscillation can begin and the photon flux Φ in the resonator can increase. As with other homogeneously broadened lasers, saturation sets in as the photon flux becomes larger and the population difference becomes depleted [see (14.1-2)]. As shown in Fig. 14.2-1, the gain coefficient then decreases until it becomes equal to the loss coefficient, whereupon steady state is reached.

As with the internal photon-flux density and the internal photon-number density considered for other types of lasers [see (14.2-2) and (14.2-13)], the steady-state internal photon flux Φ is proportional to the difference between the pumping rate R and the threshold pumping rate R_t. Since $R \propto i$ and $R_t \propto i_t$, in accordance with (16.2-8), Φ may be written as

$$\Phi = \begin{cases} \eta_i \dfrac{i - i_t}{e}, & i > i_t \\ 0, & i \le i_t. \end{cases} \tag{16.3-8}$$

Steady-State Laser Internal Photon Flux

Thus the steady-state laser internal photon flux (photons per second generated within the active region) is equal to the electron flux (which is the number of injected electrons per second) in excess of that required for threshold, multiplied by the internal quantum efficiency η_i.

The internal laser power above threshold is simply related to the internal photon flux Φ by the relation $P = h\nu\Phi$, so that we obtain

$$P = \eta_i (i - i_t) \frac{1.24}{\lambda_o}, \tag{16.3-9}$$

Internal Laser Power
λ_o (μm), P (W), i (A)

provided that λ_o is expressed in μm, i in amperes, and P in Watts.

Output Photon Flux and Efficiency

The laser output photon flux Φ_o is the product of the internal photon flux Φ and the **emission efficiency** η_e [see (14.2-16)], which is the ratio of the loss associated with the useful light transmitted through the mirrors to the total resonator loss α_r. If only the light transmitted through mirror 1 is used, then $\eta_e = \alpha_{m1}/\alpha_r$; on the other hand, if

the light transmitted through both mirrors is used, then $\eta_e = \alpha_m/\alpha_r$. In the latter case, if both mirrors have the same reflectance $\mathscr{R}$, we obtain $\eta_e = [(1/d)\ln(1/\mathscr{R})]/\alpha_r$. The laser output photon flux is therefore given by

$$\Phi_o = \eta_e \eta_i \frac{i - i_t}{e}. \tag{16.3-10}$$

Laser Output Photon Flux

It is clear from (16.3-10) that the proportionality between the laser output photon flux and the injected electron flux above threshold is governed by the **external differential quantum efficiency**

$$\eta_d = \eta_e \eta_i. \tag{16.3-11}$$

External Differential Quantum Efficiency

η_d therefore represents the rate of change of the output photon flux with respect to the injected electron flux above threshold, i.e.,

$$\eta_d = \frac{d\Phi_o}{d(i/e)}. \tag{16.3-12}$$

The laser output power above threshold is $P_o = h\nu\Phi_o = \eta_d(i - i_t)(h\nu/e)$, which may therefore be written as

$$P_o = \eta_d(i - i_t)\frac{1.24}{\lambda_o}, \tag{16.3-13}$$

Laser Output Power
λ_o (μm), P_o (W), i (A)

provided that λ_o is expressed in μm. The output power is plotted against the injected (drive) current i as the straight line in Fig. 16.3-4 with the parameters $i_t \approx 21$ mA and $\eta_d = 0.4$. This is called the **light-current curve**. The solid curve in Fig. 16.3-4 represents data obtained from both output faces of a 1.3-μm InGaAsP semiconductor

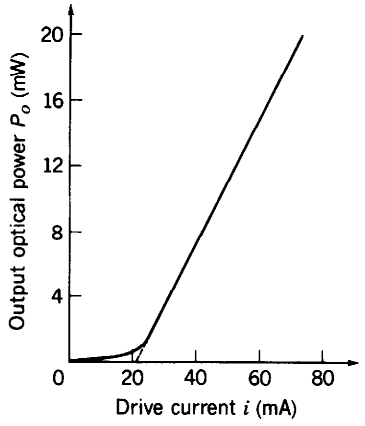

Figure 16.3-4 Ideal (straight line) and actual (solid curve) laser light-current curve for a strongly index-guided buried-heterostructure (see Fig. 16.3-7) InGaAsP injection laser operated at a wavelength of 1.3 μm. Nonlinearities, which are not accounted for by the simple theory presented here, cause the optical output power to saturate for currents greater than about 75 mA (not shown).

injection laser. The agreement between the simple theory presented here and the data is very good and shows clearly that the emitted optical power does indeed increase linearly with the drive current (over the range 23 to 73 mA in this example).

From (16.3-13) it is clear that the slope of the light-current curve above threshold is given by

$$\Re_d = \frac{dP_o}{di} = \eta_d \frac{1.24}{\lambda_o} \qquad [\lambda_o\,(\mu\text{m}), P_o\,(\text{W}), i\,(\text{A})]. \qquad (16.3\text{-}14)$$

$\Re_d$ is called the **differential responsivity** of the laser (W/A); it represents the ratio of the optical power increase to the electric current increase above threshold. For the data shown in Fig. 16.3-4, $dP_o/di \approx 0.38$ W/A.

The **overall efficiency** (power-conversion efficiency) η is defined as the ratio of the emitted laser light power to the electrical input power iV, where V is the forward-bias voltage applied to the diode. Since $P_o = \eta_d(i - i_t)(h\nu/e)$, we obtain

$$\eta = \eta_d\left(1 - \frac{i_t}{i}\right)\frac{h\nu}{eV}. \qquad (16.3\text{-}15)$$

Overall Efficiency

For operation well above threshold, which provides $i \gg i_t$, and for $eV \approx h\nu$, as is usually the case, we obtain $\eta \approx \eta_d$. The data illustrated in Fig. 16.3-4 therefore exhibit an overall efficiency $\eta \approx 40\%$, which is greater than that of any other type of laser (see Table 14.2-1). Indeed, this value is somewhat below the record high value reported to date, which is $\approx 65\%$. The electrical power that fails to be transformed into light becomes heat. Because laser diodes do, in fact, generate substantial amounts of heat they are usually mounted on heat sinks which help to dissipate the heat and stabilize the temperature.

Summary

There are four efficiencies associated with the semiconductor injection laser: the internal quantum efficiency $\eta_i = \tau_r/\tau = \tau/\tau_r$, which accounts for the fact that only a fraction of the electron–hole recombinations are radiative in nature; the emission efficiency η_e, which accounts for the fact that only a portion of the light lost from the cavity is useful; the external differential quantum efficiency $\eta_d = \eta_e\eta_i$, which accounts for both of these effects; and the power-conversion efficiency η, which is the overall efficiency. The differential responsivity $\Re_d$ (W/A) is also used as a measure of performance.

EXAMPLE 16.3-3. ***InGaAsP Double-Heterostructure Laser Diode.*** Consider again Example 16.3-2 for the InGaAsP/InP double-heterostructure semiconductor injection laser with $\eta_i = 0.5$, $\alpha_m = 59\ \text{cm}^{-1}$, $\alpha_r = 118\ \text{cm}^{-1}$, and $i_t = 38$ mA. If the light from both output faces is used, the emission efficiency is $\eta_e = \alpha_m/\alpha_r = 0.5$, while the external differential quantum efficiency is $\eta_d = \eta_e\eta_i = 0.25$. At $\lambda_o = 1.3$ μm, the differential responsivity of this laser is $dP_o/di = 0.24$ W/A. If, for example, $i = 50$ mA, we obtain $i - i_t = 12$ mA and $P_o = 12 \times 0.24 = 2.9$ mW. Comparison of these numbers with those

obtained from the data in Fig. 16.3-4 shows that the double-heterostructure laser has a higher threshold, and a lower efficiency and differential responsivity, than the buried-heterostructure laser. This illustrates the superiority of the strongly index-guided buried-heterostructure device over the strongly gain-guided double-heterostructure device.

Comparison of Laser Diode and LED Operation

Laser diodes produce light even below threshold, as is apparent from Fig. 16.3-4. This light arises from spontaneous emission, which was examined in Sec. 16.1 in connection with the LED, but which has been ignored in the present laser theory. When operated below threshold, the semiconductor laser diode acts as an edge-emitting LED. In fact, most LEDs are simply edge-emitting double-heterostructure devices. Laser diodes with sufficiently strong injection so that stimulated emission is much greater than spontaneous emission, but with little feedback so that the lasing threshold is high, are called **superluminescent LEDs.**

As discussed in Sec. 16.1, there are four efficiencies associated with the LED: the internal quantum efficiency η_i, which accounts for the fact that only a fraction of the electron–hole recombinations are radiative in nature; the transmittance efficiency η_e, which accounts for the fact that only a small fraction of the light generated in the junction region can escape from the high-index medium; the external quantum efficiency $\eta_{ex} = \eta_i \eta_e$, which accounts for both of these effects; and the power-conversion efficiency η, which is the overall efficiency. The responsivity $\mathfrak{R}$ is also used as a measure of LED performance.

There is a one-to-one correspondence between the quantities η_i, η_e, and η for the LED and the laser diode. Furthermore, there is a correspondence between η_{ex} and η_d, $\mathfrak{R}$ and $\mathfrak{R}_d$, and i and $(i - i_t)$. The superior performance of the laser results from the fact that η_e can be much greater than in the LED. This stems from the fact that the laser operates on the basis of stimulated (rather than spontaneous) emission, which has several important consequences. The stimulated emission in an above-threshold device causes the laser light rays to travel perpendicularly to the facets of the material where the loss is minimal. This provides three advantages: a net gain in place of absorption, the prevention of light rays from becoming trapped because they impinge on the inner surfaces of the material perpendicularly (and therefore at an angle less than the critical angle), and multiple opportunities for the rays to emerge as useful light from the facet as they execute multiple round trips within the cavity. LED light, by contrast, is subject to absorption and trapping and has only a single opportunity to escape; if it is not successful, it is lost. The net result is that a laser diode operated above threshold has a value of η_d (typically $\approx 40\%$) that far exceeds the value of η_{ex} (typically $\approx 2\%$) for an LED, as is evident in the comparison of Figs. 16.3-4 and 16.1-8.

C. Spectral Distribution

The spectral distribution of the laser light generated is governed by three factors, as described in Sec. 14.2B:

- The spectral width B within which the active medium small-signal gain coefficient $\gamma_0(\nu)$ is greater than the loss coefficient α_r.
- The homogeneous or inhomogeneous nature of the line-broadening mechanism (see Sec. 12.2D).
- The resonator modes, in particular the approximate frequency spacing between the longitudinal modes $\nu_F = c/2d$, where d is the resonator length.

Semiconductor lasers are characterized by the following features:

- The spectral width of the gain coefficient is relatively large because transitions occur between two energy bands rather than between two discrete energy levels.
- Because intraband processes are very fast, semiconductors tend to be homogeneously broadened. Nevertheless, spatial hole burning permits the simultaneous oscillation of many longitudinal modes (see Sec. 14.2B). Spatial hole burning is particularly prevalent in short cavities in which there are few standing-wave cycles. This permits the fields of different longitudinal modes, which are distributed along the resonator axis, to overlap less, thereby allowing partial spatial hole burning to occur.
- The semiconductor resonator length d is significantly smaller than that of most other lasers. The frequency spacing of adjacent resonator modes $\nu_F = c/2d$ is therefore relatively large. Nevertheless, many of these can generally fit within the broad band B over which the small-signal gain exceeds the loss (the number of possible laser modes is $M = B/\nu_F$).

EXAMPLE 16.3-4. ***Number of Longitudinal Modes in an InGaAsP Laser.*** An InGaAsP crystal ($n = 3.5$) of length $d = 400$ μm has resonator modes spaced by $\nu_F = c/2d = c_o/2nd \approx 107$ GHz. Near the central wavelength $\lambda_o = 1.3$ μm, this frequency spacing corresponds to a free-space wavelength spacing λ_F, where $\lambda_F/\lambda_o = \nu_F/\nu$, so that $\lambda_F = \lambda_o\nu_F/\nu = \lambda_o^2/2nd \approx 0.6$ nm. If the spectral width $B = 1.2$ THz (corresponding to a wavelength width of 7 nm), then approximately 11 longitudinal modes may oscillate. A typical spectral distribution consisting of a single transverse mode and about 11 longitudinal modes is illustrated in Fig. 16.3-5. The overall spectral width of semiconductor injection lasers is greater than that of most other lasers, particularly gas lasers (see Table 13.2-1). To reduce the number of modes to one, the resonator length d would have to be reduced so that $B = c/2d$, requiring a cavity of length $d \approx 36$ μm.

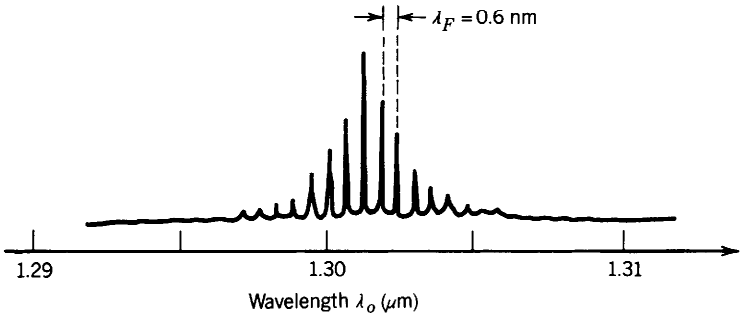

Figure 16.3-5 Spectral distribution of a 1.3-μm InGaAsP index-guided buried-heterostructure laser. This distribution is considerably narrower, and differs in shape, from that of the $\lambda_o \approx 1.3$-μm InGaAsP LED shown in Fig. 16.1-9. The number of modes decreases as the injection current increases; the mode closest to the gain maximum increases in power while the side peaks saturate. (Adapted from R. J. Nelson, R. B. Wilson, P. D. Wright, P. A. Barnes, and N. K. Dutta, CW Electrooptical Properties of InGaAsP ($\lambda = 1.3$ μm) Buried-Heterostructure Lasers, *IEEE Journal of Quantum Electronics*, vol. QE-17, pp. 202–207, © 1981 IEEE.)

The approximate linewidth of each longitudinal mode is typically ≈ 0.01 nm (corresponding to a few GHz) for gain-guided lasers, but generally far smaller (≈ 30 MHz) for index-guided lasers.

D. Spatial Distribution

Like in other lasers, oscillation in semiconductor injection lasers takes the form of transverse and longitudinal modes. In Sec. 14.2C the indices (l, m) were used to characterize the spatial distributions in the transverse direction, while the index q was used to represent variation along the direction of wave propagation or temporal behavior. In most other lasers, the laser beam lies totally within the active medium so that the spatial distributions of the different modes are determined by the shapes of the mirrors and their separations. In circularly symmetric systems, the transverse modes can be represented in terms of Laguerre–Gaussian or, more conveniently, Hermite–Gaussian beams (see Sec. 9.2D). The situation is different in semiconductor lasers since the laser beam extends outside the active layer. The transverse modes are modes of the dielectric waveguide created by the different layers of the semiconductor diode.

The transverse modes can be determined by using the theory presented in Sec. 7.3 for an optical waveguide with rectangular cross section of dimensions l and w. If l/λ_o is sufficiently small (as it usually is in double-heterostructure lasers), the waveguide will admit only a single mode in the transverse direction perpendicular to the junction plane. However, w is usually larger than λ_o, so that the waveguide will support several modes in the direction parallel to the plane of the junction, as illustrated in Fig. 16.3-6. Modes in the direction parallel to the junction plane are called **lateral modes**. The larger the ratio w/λ_o, the greater the number of lateral modes possible.

Because higher-order lateral modes have a wider spatial spread, they are less confined; their loss coefficient α_r is therefore greater than that for lower-order modes. Consequently, some of the highest-order modes will fail to satisfy the oscillation conditions; others will oscillate at a lower power than the fundamental (lowest-order) mode. To achieve high-power single-spatial-mode operation, the number of waveguide modes must be reduced by decreasing the width w of the active layer. The attendant reduction of the junction area also has the effect of reducing the threshold current.

An example of a design using a laterally confined active layer is the buried-heterostructure laser illustrated in Fig. 16.3-7. The lower-index material on either side of the active region produces lateral confinement in this (and other laterally confined) index-guided lasers.

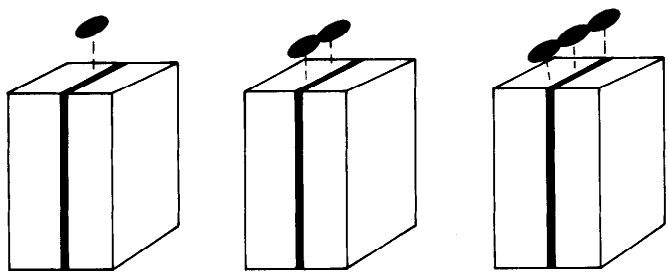

Figure 16.3-6 Schematic illustration of spatial distributions of the optical intensity for the laser waveguide modes $(l, m) = (1, 1)$, $(1, 2)$, and $(1, 3)$.

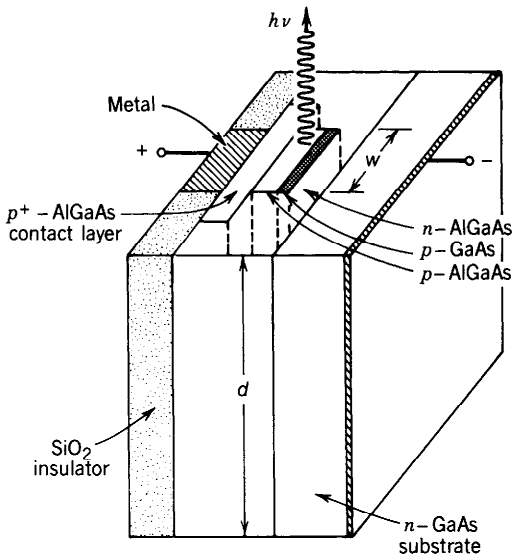

Figure 16.3-7 Schematic diagram of an AlGaAs/GaAs buried-heterostructure semiconductor injection laser. The junction width w is typically 1 to 3 μm, so that the device is strongly index guided.

Far-Field Radiation Pattern

A laser diode with an active layer of dimensions l and w emits light with far-field angular divergence $\approx \lambda_o/l$ (radians) in the plane perpendicular to the junction and $\approx \lambda_o/w$ in the plane parallel to the junction (see Fig. 16.3-8). (Recall from Sec. 3.1B, for example, that for a Gaussian beam of diameter $2W_0$ the divergence angle is $\theta \approx (2/\pi)(\lambda_o/2W_0) = \lambda_o/\pi W_0$ when $\theta \ll 1$). The angular divergence determines the far-field radiation pattern (see Sec. 4.3). Because of its small active layer, the semicon-

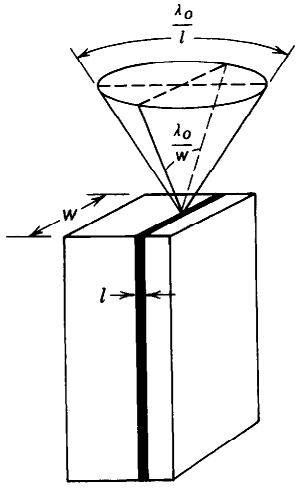

Figure 16.3-8 Angular distribution of the optical beam emitted from a laser diode.

ductor injection laser is characterized by an angular divergence larger than that of most other lasers. As an example, if $l = 2$ μm, $w = 10$ μm, and $\lambda_o = 0.8$ μm, the divergence angles are calculated to be $\approx 23°$ and 5°. Light from a single-transverse-mode laser diode, for which w is smaller, has an even larger angular divergence. The spatial distribution of the far-field light within the radiation cone depends on the number of transverse modes and on their optical powers. The highly asymmetric elliptical distribution of laser-diode light can make its collimation tricky.

E. Mode Selection

Single-Frequency Operation

As indicated above, a semiconductor injection laser may be operated on a single-transverse mode by reducing the dimensions of the active-layer cross section (l and w), so that it acts as a single-mode waveguide. Single-frequency operation may be achieved by reducing the length d of the resonator so that the frequency spacing between adjacent longitudinal modes exceeds the spectral width of the amplifying medium.

Other methods of single-mode operation include the use of multiple-mirror resonators, as discussed in Sec. 14.2D and illustrated in Fig. 14.2-15. A double-resonator diode laser (coupled-cavity laser) can be implemented by cleaving a groove perpendicular to the active layer, as shown in Fig. 16.3-9. This creates two coupled cavities so that the structure is known as a **cleaved-coupled-cavity** (C^3) **laser**. The standing wave in the laser must satisfy boundary conditions at the surfaces of both cavities, thereby providing a more stringent restriction that can be satisfied only at a single frequency. In practice, the usefulness of this approach is limited by thermal drift.

An alternative approach is to replace the cleaved surfaces usually used as mirrors with frequency-selective reflectors such as gratings parallel to the junction plane [Fig. 16.3-10(a)]. The grating is a periodic structure that reflects light only when the grating period Λ satisfies $\Lambda = q\lambda/2$, where q is an integer (see Sec. 2.4B). These are called **distributed Bragg reflectors** and the device is known as a DBR laser.

Yet another approach places the grating itself directly adjacent to the active layer by using a spatially corrugated waveguide as shown in Fig. 16.3-10(b). The grating then acts as a distributed reflector, substituting for the lumped reflections provided by the mirrors of a Fabry–Perot laser. The surfaces of the crystal are antireflection coated to minimize surface reflections. This structure is known as a **distributed-feedback** (DFB) **laser**. DFB lasers operate with spectral widths as small as 10 MHz (without modulation) and offer modulation bandwidths well into the GHz range. They are used in many

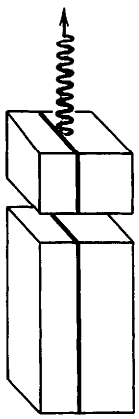

Figure 16.3-9 Cleaved-coupled-cavity (C^3) laser.

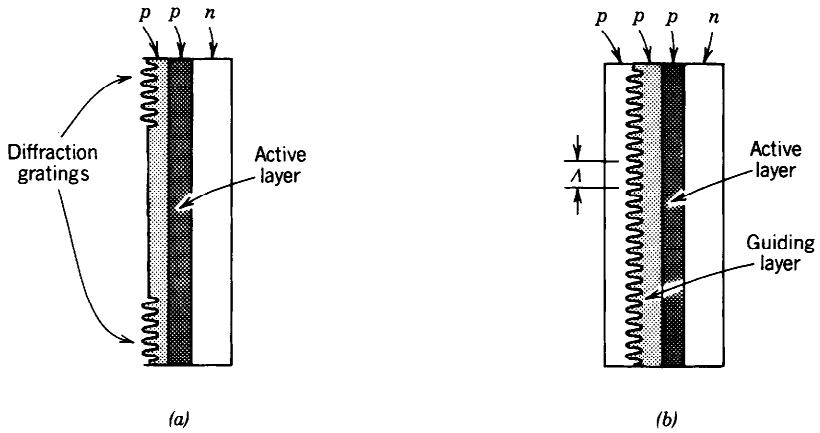

Figure 16.3-10 (*a*) External diffraction gratings serve as mirrors in a DBR laser. (*b*) The distributed feedback (DFB) laser has a periodic layer that acts as a distributed reflector.

applications including fiber-optic communications in the wavelength range 1.3 to 1.55 μm.

F. Characteristics of Typical Lasers

Semiconductor lasers have been operated at wavelengths stretching from the near ultraviolet to the far infrared, as illustrated in Fig. 16.3-11. They have been operated with power outputs reaching 100 mW, but laser-diode arrays (with closely spaced active regions) offer narrow coherent beams with powers in excess of 10 W. Surface-emitting laser diodes (SELDs) are becoming increasingly common.

Laser diodes operating in the visible band are usually fabricated from $Ga_{0.5}In_{0.5}P$ and generate light at $\lambda_o \approx 670$ nm. They use either gain-guided or index-guided structures. CW output powers are typically ≈ 5 mW at $T = 300$ K; an off-the-shelf device might operate at a voltage of 2.1 V and a current of 85 mA. Powers as high as 50 mW have been achieved using index-guided lateral confinement. The efficiency of a GaInP laser is substantially greater, and the size substantially smaller, than a 5-mW He–Ne laser operating at 633 nm. Room-temperature CW lasers operating at 584 nm (in the yellow) can be fabricated by using AlInP instead of GaInP.

In the near infrared, direct-bandgap ternary and quaternary materials are often used because their wavelengths can be compositionally tuned and CW operation at room temperature is possible. Temperature tuning can be used to adjust the output wavelength on a fine scale. As with LEDs, $Al_xGa_{1-x}As$ ($\lambda_o = 0.75$ to 0.87 μm) and $In_{1-x}Ga_xAs_{1-y}P_y$ ($\lambda_o = 1.1$ to 1.6 μm) are particularly important.

Laser diodes can also be operated throughout the middle-infrared region, although cooling is then required for efficient operation. II–VI direct-gap compounds such as $Hg_xCd_{1-x}Te$, and IV–VI materials such as $Pb_xSn_{1-x}Te$, are used over a broad range of this region from about 3 to 35 μm. When operated at very low temperatures, $Bi_{1-x}Sb_x$ lases out to wavelengths as long as ≈ 100 μm.

*G. Quantum-Well Lasers

As emphasized earlier, the laser threshold current density may be reduced by decreasing the thickness of the active layer. We have already discussed the way that heterostructures are used to confine electrons and photons within the active layer. When

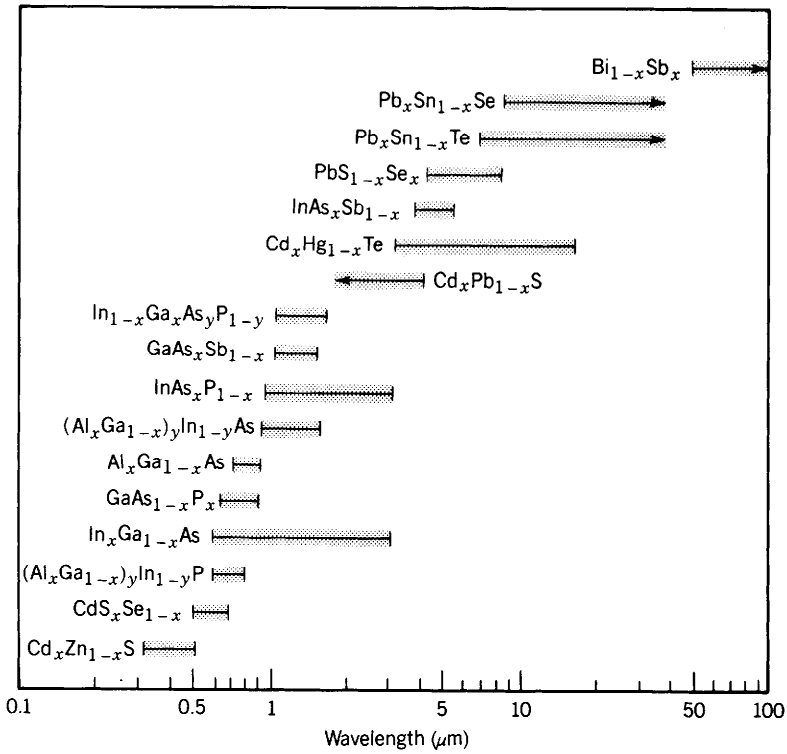

Figure 16.3-11 Compound materials used for semiconductor lasers. The range of wavelengths reaches from the near ultraviolet to the far infrared. Semiconductor lasers operating at $\lambda_o > 3$ μm usually require cooling below $T = 300$ K. Some of these materials require optical or electron-beam pumping to lase.

the thickness of the active layer is made sufficiently narrow (i.e., smaller than the dc Broglie wavelength of a thermalized electron), quantum effects begin to play a dramatic role. Since the active layer in a double heterostructure has a bandgap energy smaller than the surrounding layers, the structure then acts as a quantum well (see Sec. 15.1G) and the laser is called a single-quantum well (SQW) laser or simply a quantum-well laser.

The band structure and energy–momentum (E–k) relations of a quantum well are different from bulk material. The conduction band is split into a number of subbands, labeled by the quantum number $q = 1, 2, \ldots$, each with its own energy–momentum relation and density of states. The bottoms of these subbands have energies $E_c + E_q$, where $E_q = \hbar^2(q\pi/l)^2/2m_c$, $q = 1, 2, \ldots$, are the energies of an electron of effective mass m_c in a one-dimensional quantum well of thickness l (see Figs. 15.1-21 and 15.1-22; q_1 and d_1 in Chap. 15 correspond to q and l here). Each subband has a parabolic E–k relation and a constant density of states that is independent of energy. The overall density of states in the conduction band, $\varrho_c(E)$, therefore assumes a staircase distribution [see (15.1-28)] with steps at energies $E_c + E_q$, $q = 1, 2, \ldots$. The valence band has similar subbands at energies $E_v - E'_q$, where $E'_q = \hbar^2(q\pi/l)^2/2m_v$ are the energies of a hole of effective mass m_v in a quantum well of thickness l.

The interactions of photons with electrons and holes in a quantum well take the form of energy- and momentum-conserving transitions between the conduction and valence bands. The transitions must also conserve the quantum number q, as illustrated in Fig. 16.3-12; they obey rules similar to those that govern transitions between

the conduction and valence bands in bulk semiconductors. The expressions for the transition probabilities and gain coefficient in the bulk material (see Sec. 15.2) apply to the quantum-well structure if we simply replace the bandgap energy E_g with the energy gap between the subbands, $E_{gq} = E_g + E_q + E'_q$, and use a constant density of states rather than one that varies as the square root of energy. The total gain coefficient is the sum of the gain coefficients provided by all of the subbands ($q = 1, 2, \ldots$).

Density of States

Consider transitions between the two subbands of quantum number q. To satisfy the conservation of energy and momentum, a photon of energy $h\nu$ interacts with states of energies $E = E_c + E_q + (m_r/m_c)(h\nu - E_{gq})$ in the upper subband and $E - h\nu$ in the lower. The optical joint density of states $\varrho(\nu)$ is related to $\varrho_c(E)$ by $\varrho(\nu) = (dE/d\nu)\varrho_c(E) = (hm_r/m_c)\varrho_c(E)$. It follows from (15.1-28) that

$$\varrho(\nu) = \begin{cases} \dfrac{hm_r}{m_c}\dfrac{m_c}{\pi\hbar^2 l} = \dfrac{2m_r}{\hbar l}, & h\nu > E_g + E_q + E'_q \\ 0, & \text{otherwise.} \end{cases} \tag{16.3-16}$$

Including transitions between all subbands $q = 1, 2, \ldots$, we arrive at a $\varrho(\nu)$ that has a staircase distribution with steps at the energy gaps between subbands of the same quantum number (Fig. 16.3-12).

Gain Coefficient

The gain coefficient of the laser is given by the usual expression [see (15.2-23)]

$$\gamma_0(\nu) = \frac{\lambda^2}{8\pi\tau_r}\varrho(\nu)f_g(\nu), \tag{16.3-17}$$

where the Fermi inversion factor $f_g(\nu)$ depends on the quasi-Fermi levels and tempera-

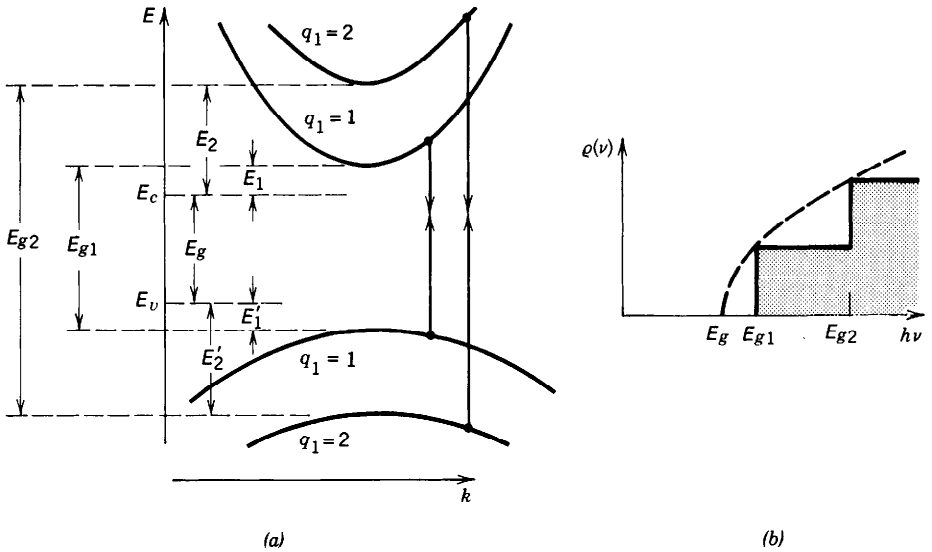

Figure 16.3-12 (*a*) E–k relations of different subbands. (*b*) Optical joint density of states for a quantum-well structure (staircase curve) and for a bulk semiconductor (dashed curve). The first jump occurs at energy $E_{g1} = E_g + E_1 + E'_1$ (where E_1 and E'_1 are, respectively, the lowest energies of an electron and a hole in the quantum well).

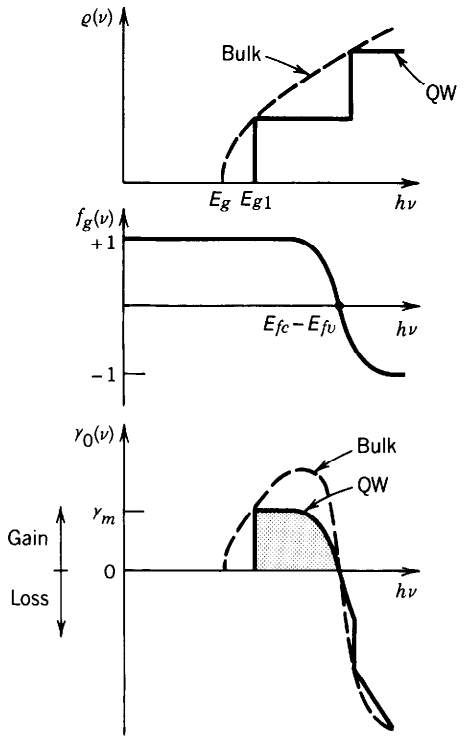

Figure 16.3-13 Density of states $\rho(\nu)$, Fermi inversion factor $f_g(\nu)$, and gain coefficient $\gamma_0(\nu)$ in quantum-well (solid-curves) and bulk (dashed curves) structures.

ture and is the same for bulk and quantum-well lasers. The density of states $\rho(\nu)$, however, differs in the two cases as we have shown. The frequency dependences of $\rho(\nu)$, $f_g(\nu)$, and their product are illustrated in Fig. 16.3-13 for quantum-well and bulk double-heterostructure configurations. The quantum-well laser has a smaller peak gain and a narrower gain profile.

It is assumed in Fig. 16.3-13 that only a single step of the staircase function $\rho(\nu)$ occurs at an energy smaller than $E_{fc} - E_{fv}$. This is the case under usual injection conditions. The maximum gain γ_m may then be determined by substituting $f_g(\nu) = 1$ and $\rho(\nu) = 2m_r/\hbar l$ in (16.3-17), yielding

$$\gamma_m = \frac{\lambda^2 m_r}{2\tau_r h l}. \tag{16.3-18}$$

Relation Between Gain Coefficient and Current Density

By increasing the injected current density J, the concentration of excess electrons and holes Δn is increased and, therefore, so is the separation between the quasi-Fermi levels $E_{fc} - E_{fv}$. The effect of this increase on the gain coefficient $\gamma_0(\nu)$ may be assessed by examining the diagrams in Fig. 16.3-13. For sufficiently small J there is no gain. When J is such that $E_{fc} - E_{fv}$ just exceeds the gap E_{g1} between the $q = 1$ subbands, the medium provides gain. The peak gain coefficient increases sharply and saturates at the value γ_m. A further increase of J increases the gain spectral width but not its peak value. If J is increased yet further, to the point where $E_{fc} - E_{fv}$ exceeds the gap E_{g2} between the $q = 2$ subbands, the peak gain coefficient undergoes another jump, and so on. The gain profile can therefore be quite broad, providing the possibility of a wide tuning range for such lasers. The dependences of γ_p on J for quantum-well and bulk double-heterostructure semiconductor lasers are illustrated schematically in

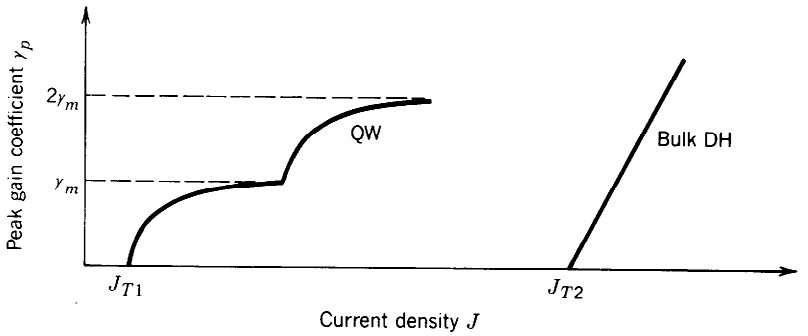

Figure 16.3-14 Schematic relations between peak gain coefficient γ_p and current density J in quantum-well (QW) and bulk double-heterostructure (DH) lasers.

Fig. 16.3-14. The quantum-well laser has a far smaller value of J_T (current density required for transparency), but its gain saturates at a lower value.

The threshold current density for QW laser oscillation is considerably smaller than that for bulk (DH) laser oscillation because of the reduction in active-layer thickness. Additional factors that make quantum-well lasers attractive include the narrower spectrum of the gain coefficient, the smaller linewidth of the laser modes, the possibility of achieving higher modulation frequencies, and the reduced temperature dependence.

The active-layer thickness of a SQW laser is typically < 10 nm, which is to be compared with 100 nm for a DH laser and 2 μm for an old-fashioned homojunction semiconductor laser. SQW threshold currents are roughly ≈ 0.5 mA, as compared with 20 mA for DH lasers (see Fig. 16.3-4). The spectral width of the light emitted from a SQW laser is usually < 10 MHz, which is substantially narrower than that from DH lasers. The output power of single quantum-well lasers is limited to about 100 mW to avoid facet damage. However, arrays of AlGaAs/GaAs quantum-well lasers can emit as much as 50 W of incoherent CW optical power in a line of dimensions 1 μm $\times$ 1 cm, making them excellent candidates for the side-pumping of solid-state lasers such as Nd^{3+}:YAG (see Sec. 13.2). Remarkably, the overall quantum efficiency η of such arrays is $> 50\%$ and the differential quantum efficiency η_d can exceed 80%.

Semiconductor lasers have also been fabricated in quantum-wire configurations (see Sec. 15.1G). Threshold currents < 0.1 mA are expected for devices in which l and w are both ≈ 10 nm. Arrays of quantum-dot lasers would offer yet lower threshold currents.

Multiquantum-Well Lasers

The gain coefficient may be increased by using a parallel stack of quantum wells. This structure, illustrated in Fig. 16.3-15, is known as a multiquantum-well (MQW) laser. The gain of an N-well MQW laser is N times the gain of each of its wells. However, a fair comparison of the performance of single quantum-well (SQW) and MQW lasers requires that both be injected by the same current. Assume that a single quantum well is injected with an excess carrier density Δn and has a peak gain coefficient γ_p. Each of the N wells in the MQW structure would then be injected with only $\Delta n/N$ carriers. Because of the nonlinear dependence of the gain on Δn, the gain coefficient of each well is $\xi\gamma_p/N$, where ξ may be smaller or greater than 1, depending on the operating conditions. The total gain provided by the MQW laser is $N(\xi\gamma_p/N) = \xi\gamma_p$. It is not clear which of the two structures produces higher gain. It turns out that at low current densities, the SQW is superior, while at high current densities, the MQW is superior (but by a factor of less than N).

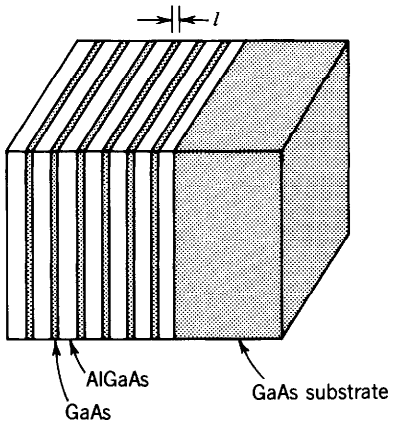

Figure 16.3-15 An AlGaAs/GaAs multiquantum-well laser with $l = 10$ nm.

Strained-Layer Lasers

Surprising as it may seem, the introduction of strain can provide a salutatory effect on the performance of semiconductor injection lasers. **Strained-layer lasers** can have superior properties, and can operate at wavelengths other than those accessible by means of compositional tuning. These lasers have been fabricated from III–V semiconductor materials, using both single-quantum-well and multiquantum-well configurations. Rather than being lattice-matched to the confining layers, the active layer is purposely chosen to have a different lattice constant. If sufficiently thin, it can accommodate its atomic spacings to those of the surrounding layers, and in the process become strained (if the layer is too thick it will not properly accommodate and the material will contain dislocations). The InGaAs active layer in an InGaAs/AlGaAs strained-layer laser, for example, has a lattice constant that is significantly greater than that of its AlGaAs confining layers. The thin InGaAs layer therefore experiences a biaxial compression in the plane of the layer, while its atomic spacings are increased above their usual values in the direction perpendicular to the layer.

The compressive strain alters the band structure in three significant ways: (1) it increases the bandgap E_g; (2) it removes the degeneracy at $k = 0$ between the heavy and light hole bands; and (3) it makes the valence bands anisotropic so that in the direction parallel to the plane of the layer the highest band has a light effective mass, whereas in the perpendicular direction the highest band has a heavy effective mass.

This behavior can significantly improve the performance of lasers. First, the laser wavelength is altered by virtue of the dependence of E_g on the strain. Second, the laser threshold current density can be reduced by the presence of the strain. Achieving a population inversion requires that the separation of the quasi-Fermi levels be greater than the bandgap energy, i.e., $E_{fc} - E_{fv} > E_g$. The reduced hole mass more readily allows E_{fv} to descend into the valence band, thereby permitting this condition to be satisfied at a lower injection current.

Strained-layer InGaAs lasers have been fabricated in many different configurations using a variety of confining materials, including AlGaAs and InGaAsP. They have been operated over a broad range of wavelengths from 0.9 to 1.55 μm. In one particular example that uses a MQW configuration, a device constructed of several 2-nm-thick $In_{0.78}Ga_{0.22}As$ quantum-well layers, separated by 20-nm barriers and 40-nm confining layers of InGaAsP, operates at $\lambda_o = 1.55$ μm with a sub-milliampere threshold current. As another example, GaInP/InGaAlP strained-layer quantum-well lasers emit more than $\frac{1}{2}$ W at 634 nm.

Surface-Emitting Quantum-Well Laser-Diode Arrays

Surface-emitting quantum-well laser diodes (SELDs) are of increasing interest, and offer the advantages of high packing densities on a wafer scale. An array of about 1

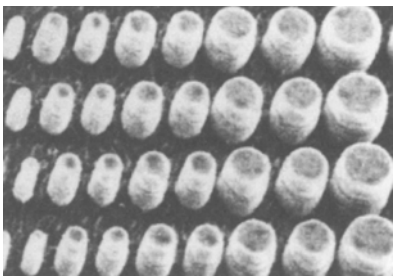

Figure 16.3-16 Scanning electron micrograph of a small portion of an array of vertical-cavity quantum-well lasers with diameters between 1 and 5 μm. (After J. L. Jewell *et al.*, Low Threshold Electrically-Pumped Vertical-Cavity Surface-Emitting Micro-Lasers, *Optics News*, vol. 15, no. 12, pp. 10–11, 1989.)

million electrically pumped tiny vertical-cavity cylindrical $In_{0.2}Ga_{0.8}As$ quantum-well SELDs (diameter ≈ 2 μm, height ≈ 5.5 μm), with lasing wavelengths in the vicinity of 970 nm, has been fabricated on a single 1-cm^2 chip of GaAs. These particular devices have thresholds $i_t \approx 1.5$ mA, for $T = 300$ K CW operation, and single-facet external differential quantum efficiencies $\eta_d \approx 16\%$. A scanning electron micrograph of a small portion of such an array is shown in Fig. 16.3-16. The circular output beams have the advantage of providing easy coupling to optical fibers. More recently, the lasing thresholds of devices of this type have been reduced to ≈ 0.2 mA. Their very small active-material volume (≈ 0.05 μm^3) can, in principle, permit thresholds as low as 10 μA.

READING LIST

Books and Articles on Laser Theory

See the reading list in Chapter 13.

Books and Articles on Semiconductor Physics

See the reading list in Chapter 15.

Books on LEDs and Semiconductor Injection Lasers

Y. Yamamoto, ed., *Coherence, Amplification, and Quantum Effects in Semiconductor Lasers*, Wiley, New York, 1991.

P. K. Cheo, ed., *Handbook of Solid-State Lasers*, Marcel Dekker, New York, 1988.

G. P. Agrawal and N. K. Dutta, *Long-Wavelength Semiconductor Lasers*, Van Nostrand Reinhold, New York, 1986.

R. K. Willardson and A. C. Beer, eds., *Semiconductors and Semimetals*, vol. 22, *Lightwave Communications Technology*, W. T. Tsang, ed., part B, *Semiconductor Injection Lasers, I*, Academic Press, New York, 1985.

R. K. Willardson and A. C. Beer, eds., *Semiconductors and Semimetals*, vol. 22, *Lightwave Communications Technology*, W. T. Tsang, ed., part C, *Semiconductor Injection Lasers, II and Light Emitting Diodes*, Academic Press, New York, 1985.

H. Kressel, ed., *Semiconductor Devices for Optical Communication*, Springer-Verlag, Berlin, 2nd ed. 1982.

G. H. B. Thomson, *Physics of Semiconductor Lasers*, Wiley, New York, 1981.

H. C. Casey, Jr., and M. B. Panish, *Heterostructure Lasers*, part A, *Fundamental Principles*, Academic Press, New York, 1978.

H. C. Casey, Jr., and M. B. Panish, *Heterostructure Lasers*, part B, *Materials and Operating Characteristics*, Academic Press, New York, 1978.

H. Kressel and J. K. Butler, *Semiconductor Lasers and Heterojunction LEDs*, Academic Press, New York, 1977.

E. W. Williams and R. Hall, *Luminescence and the Light Emitting Diode*, Pergamon Press, New York, 1977.

A. A. Bergh and P. J. Dean, *Light Emitting Diodes*, Clarendon Press, Oxford, 1976.

C. H. Gooch, *Injection Electroluminescent Devices*, Wiley, New York, 1973.

R. W. Campbell and F. M. Mims III, *Semi-Conductor Diode Lasers*, Howard Sams, Indianapolis, IN, 1972.

Special Journal Issues

Special issue on laser technology, *Lincoln Laboratory Journal*, vol. 3, no. 3, 1990.

Special issue on semiconductor diode lasers, *IEEE Journal of Quantum Electronics*, vol. QE-25, no. 6, 1989.

Special issue on semiconductor lasers, *IEEE Journal of Quantum Electronics*, vol. QE-23, no. 6, 1987.

Special issue on semiconductor quantum wells and superlattices: physics and applications, *IEEE Journal of Quantum Electronics*, vol. QE-22, no. 9, 1986.

Special issue on semiconductor lasers, *IEEE Journal of Quantum Electronics*, vol. QE-21, no. 6, 1985.

Special issue on optoelectronics, *Physics Today*, vol. 38, no. 5, 1985.

Special issue on light emitting diodes and long-wavelength photodetectors, *IEEE Transactions on Electron Devices*, vol. ED-30, no. 4, 1983.

Special issue on optoelectronic devices, *IEEE Transactions on Electron Devices*, vol. ED-29, no. 9, 1982.

Special issue on light sources and detectors, *IEEE Transactions on Electron Devices*, vol. ED-28, no. 4, 1981.

Special issue on quaternary compound semiconductor materials and devices—sources and detectors, *IEEE Journal of Quantum Electronics*, vol. QE-17, no. 2, 1981.

Special joint issue on optoelectronic devices and circuits, *IEEE Transactions on Electron Devices*, vol. ED-25, no. 2, 1978.

Special issue on semiconductor lasers, *IEEE Journal of Quantum Electronics*, vol. QE-6, no. 6, 1970.

Articles

J. Jewell, Surface-Emitting Lasers: A New Breed, *Physics World*, vol. 3, no. 7, pp. 28–30, 1990.

R. Baker, Optical Amplification, *Physics World*, vol. 3, no. 3, pp. 41–44, 1990.

D. A. B. Miller, Optoelectronic Applications of Quantum Wells, *Optics and Photonics News*, vol. 1, no. 2, pp. 7–15, 1990.

J. L. Jewell, A. Scherer, S. L. McCall, Y. H. Lee, S. J. Walker, J. P. Harbison, and L. T. Florez, Low Threshold Electrically-Pumped Vertical-Cavity Surface-Emitting Micro-Lasers, *Optics News*, vol. 15, no. 12, pp. 10–11, 1989.

A. Yariv, Quantum Well Semiconductor Lasers Are Taking Over, *IEEE Circuits and Devices Magazine*, vol. 5, no. 6, pp. 25–28, 1989.

G. Eisenstein, Semiconductor Optical Amplifiers, *IEEE Circuits and Devices Magazine*, vol. 5, no. 4, pp. 25–30, 1989.

D. Welch, W. Streifer, and D. Scifres, High Power, Coherent Laser Diodes, *Optics News*, vol. 15, no. 3, pp. 7–10, 1989.

G. P. Agrawal, Single-Longitudinal-Mode Semiconductor Lasers, in *Progress in Optics*, E. Wolf, ed., vol. 26, North-Holland, Amsterdam, 1988.

M. Ohtsu and T. Tako, Coherence in Semiconductor Lasers, in *Progress in Optics*, E. Wolf, ed., vol. 25, North-Holland, Amsterdam, 1988.

I. Hayashi, Future Prospects of the Semiconductor Laser, *Optics News*, vol. 14, no. 10, pp. 7–12, 1988.

M. Ettenberg, Laser Diode Systems and Devices, *IEEE Circuits and Devices Magazine*, vol. 3, no. 5, pp. 22–26, 1987.

G. L. Harnagel, W. Streifer, D. R. Scifres, and D. F. Welch, Ultrahigh-Power Semiconductor Diode Laser Arrays, *Science*, vol. 237, pp. 1305–1309, 1987.

Y. Suematsu, Advances in Semiconductor Lasers, *Physics Today*, vol. 38, no. 5, pp. 32–39, 1985.

D. Botez, Laser Diodes are Power-Packed, *IEEE Spectrum*, vol. 22, no. 6, pp. 43–53, 1985.

A. Mooradian, Laser Linewidth, *Physics Today*, vol. 38, no. 5, pp. 42–48, 1985.

W. T. Tsang, The C^3 Laser, *Scientific American*, vol. 251, no. 5, pp. 149–161, 1984.

S. Kobayashi and T. Kimura, Semiconductor Optical Amplifiers, *IEEE Spectrum*, vol. 21, no. 5, pp. 26–33, 1984.

F. Stern, Semiconductor Lasers: Theory, in *Laser Handbook*, F. T. Arecchi and E. O. Schultz-Du Bois, eds., North-Holland, Amsterdam, 1972.

Historical

R. D. Dupuis, An Introduction to the Development of the Semiconductor Laser, *IEEE Journal of Quantum Electronics*, vol. QE-23, pp. 651–657, 1987.

N. G. Basov, Quantum Electronics at the P. N. Lebedev Physics Institute of the Academy of Sciences of the USSR (FIAN), *Soviet Physics–Uspekhi*, vol. 29, pp. 179–185, 1986 [*Uspekhi Fizicheskikh Nauk*, vol. 148, pp. 313–324, 1986].

J. K. Butler, ed., *Semiconductor Injection Lasers*, IEEE Press, New York, 1980.

N. G. Basov, Semiconductor Lasers, in *Nobel Lectures in Physics, 1963–1970*, Elsevier, Amsterdam, 1972.

T. M. Quist, R. H. Rediker, R. J. Keyes, W. E. Krag, B. Lax, A. L. McWhorter, and H. J. Zeiger, Semiconductor Maser of GaAs, *Applied Physics Letters*, vol. 1, pp. 91–92, 1962.

N. Holonyak, Jr., and S. F. Bevacqua, Coherent (Visible) Light Emission from $Ga(As_{1-x}P_x)$ Junctions, *Applied Physics Letters*, vol. 1, pp. 82–83, 1962.

M. I. Nathan, W. P. Dumke, G. Burns, F. H. Dill, Jr., and G. Lasher, Stimulated Emission of Radiation from GaAs *p–n* Junctions, *Applied Physics Letters*, vol. 1, pp. 62–64, 1962.

R. N. Hall, G. E. Fenner, J. D. Kingsley, T. J. Soltys, and R. O. Carlson, Coherent Light Emission from GaAs Junctions, *Physical Review Letters*, vol. 9, pp. 366–368, 1962.

R. J. Keyes and T. M. Quist, Recombination Radiation Emitted by Gallium Arsenide, *Proceedings of the IRE*, vol. 50, pp. 1822–1823, 1962.

N. G. Basov, O. N. Krokhin, and Yu. M. Popov, Production of Negative-Temperature States in *p–n* Junctions of Degenerate Semiconductors, *Soviet Physics–JETP*, vol. 13, pp. 1320–1321, 1961 [*Zhurnal Eksperimental'noi i Teoreticheskoi Fiziki* (*USSR*), vol. 40, pp. 1879–1880, 1961].

M. G. A. Bernard and G. Duraffourg, Laser Conditions in Semiconductors, *Physica Status Solidi*, vol. 1, pp. 699–703, 1961.

J. von Neumann, in unpublished calculations sent to E. Teller in September 1953, showed that it was in principle possible to upset the equilibrium concentration of carriers in a semiconductor and thereby obtain light amplification by stimulated emission, e.g., from the recombination of electrons and holes injected into a *p–n* junction [see J. von Neumann, Notes on the Photon-Disequilibrium-Amplification Scheme (JvN), Sept. 16, 1953, *IEEE Journal of Quantum Electronics*, vol. QE-23, pp. 658–673, 1987].

PROBLEMS

16.1-1 **LED Spectral Widths.** Estimate the spectral widths of the $In_{0.72}Ga_{0.28}As_{0.6}P_{0.4}$, GaAs, and $GaAs_{0.6}P_{0.4}$ LEDs from the spectra provided in Fig. 16.1-9, in units of nm, Hz, and eV. Compare these estimates with the results calculated from the formulas given in Exercise 16.1-3.

16.1-2 **External Quantum Efficiency of an LED.** Derive an expression for η_e, the efficiency for the extraction of internal unpolarized light from an LED, that includes the angular dependence of Fresnel reflection at the semiconductor–air boundary (see Sec. 6.2).

16.1-3 **Coupling Light from an LED into an Optical Fiber.** Calculate the fraction of optical power emitted from an LED that is accepted by a step-index optical fiber of numerical aperture NA = 0.1 in air and core refractive index 1.46 (see Sec. 8.1). Assume that the LED has a planar surface, a refractive index $n = 3.6$, and an

angular dependence of optical power that is proportional to $\cos^4(\theta)$. Assume further that the LED is bonded to the core of the fiber and that the emission area is smaller than the fiber core.

16.2-1 **Bandwidth of Semiconductor Laser Amplifier.** Use the data in Fig. 16.2-3(a) to plot the full bandwidth of the InGaAsP amplifier against the injected carrier concentration Δn. Find an approximate linear formula for this bandwidth as a function of Δn and plot the amplifier gain coefficient versus bandwidth.

16.2-2 **Peak Gain Coefficient at $T = 0$ K.** (a) Show that the peak value γ_p of the gain coefficient $\gamma_0(\nu)$ at $T = 0$ K is located at $\nu = (E_{fc} - E_{fv})/h$.
(b) Obtain an analytic expression for the peak gain coefficient γ_p as a function of the injected carrier concentration Δn at $T = 0$ K.
(c) Plot γ_p versus Δn for an InGaAsP amplifier ($\lambda_o = 1.3$ μm, $n = 3.5$, $\tau_r = 2.5$ ns, $m_c = 0.06m_0$, $m_v = 0.4m_0$) for values of Δn in the range 1×10^{18} to 2×10^{18} cm^{-3}.
(d) Compare the results with the data provided in Fig. 16.2-3b.

*16.2-3 **Gain Coefficient of a GaAs Amplifier.** A room-temperature ($T = 300$ K) p-type GaAs laser amplifier ($E_g \approx 1.40$ eV, $m_c = 0.07m_0$, $m_v = 0.5m_0$), with refractive index $n = 3.6$, is doped ($p_0 = 1.2 \times 10^{18}$) such that the radiative recombination lifetime $\tau_r \approx 2$ ns.
(a) Given the steady-state injected-carrier concentration Δn (which is controlled by the injection rate R and the overall recombination time τ), use (16.2-2)–(16.2-4) to compute the gain coefficient $\gamma_0(\nu)$ versus the photon energy $h\nu$, assuming that $T = 0$ K.
(b) Carry out the same calculation using a computer, assuming that $T = 300$ K.
(c) Plot the peak gain coefficient as a function of Δn for both cases.
(d) Determine the loss coefficient α and the transparency concentration Δn_T using the linear approximation model.
(e) Plot the full amplifier bandwidth (in Hz, nm, and eV) as a function of Δn for both cases.
(f) Compare your results with the gain coefficient and peak gain coefficient curves calculated by Panish and shown in Fig. P16.2-3.

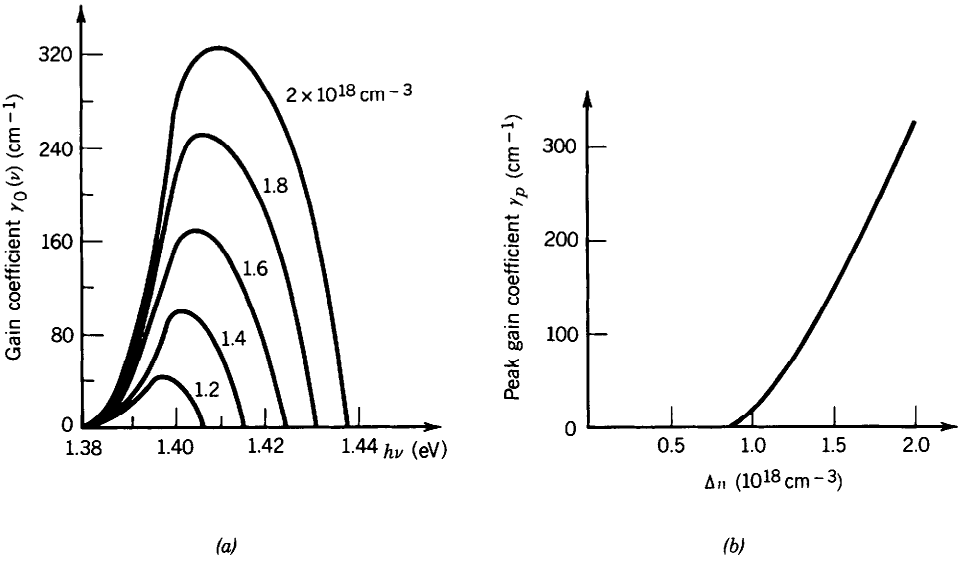

Figure P16.2-3 (Adapted from M. B. Panish, Heterostructure Injection Lasers, *Proceedings of the IEEE*, vol. 64, pp. 1512–1540, © 1976 IEEE).

16.2-4 **Bandgap Reduction Arising from Band-Tail States.** The bandgap reduction ΔE_g arising from band-tail states in InGaAsP and GaAs can be empirically expressed as

$$\Delta E_g(\text{eV}) \approx (-1.6 \times 10^{-8})(p^{1/3} + n^{1/3}),$$

where n and p are the carrier concentrations (cm^{-3}) provided by doping, carrier injection, or both.
(a) For p-type InGaAsP and GaAs, determine the concentration p that reduces the bandgap by approximately 0.02 eV.
(b) For undoped InGaAsP and GaAs, determine the injected carrier density Δn that reduces the bandgap by approximately 0.02 eV. Assume that n_i is negligible.
(c) Compute $E_g + \Delta E_g$ and compare the result with the energy at which the gain coefficient in Fig. 16.2-3(a) is zero on the low-frequency side.

16.2-5 **Amplifier Gain and Bandwidth.** GaAs has an intrinsic carrier concentration $n_i = 1.8 \times 10^6$ cm^{-3}, a recombination lifetime $\tau = 50$ ns, a bandgap energy $E_g = 1.42$ eV, an effective electron mass $m_c = 0.07m_0$, and an effective hole mass $m_v = 0.5m_0$. Assume that $T = 0$ K.
(a) Determine the center frequency, bandwidth, and peak net gain within the bandwidth for a GaAs amplifier of length $d = 200$ μm, width $w = 10$ μm, and thickness $l = 2$ μm, when 1 mA of current is passed through the device.
(b) Determine the number of voice messages that can be supported by the bandwidth determined above, given that each message occupies a bandwidth of 4 kHz.
(c) Determine the bit rate that can be passed through the amplifier given that each voice channel requires 64 kbits/s.

16.2-6 **Transition Cross Section.** Determine the transition cross section $\sigma(\nu)$ for GaAs as a function of Δn at $T = 0$ K. The transition probability is $\phi\sigma(\nu)$, where ϕ is the photon-flux density. Why is the transition cross section less useful for semiconductor laser amplifiers than for other laser amplifiers?

*16.2-7 **Gain Profile.** Consider a 1.55-μm InGaAsP amplifier ($n = 3.5$) of the configuration shown in Fig. 16.2-6, with identical antireflection coatings on its input and output facets. Calculate the maximum reflectivity of each of the facets that can be tolerated if it is desired to maintain the variations in the gain profile arising from the frequency dependence of the Fabry–Perot transmittance to less than 10% [see (9.1-29)].

16.3-1 **Dependence of Output Power on Refractive Index.** Identify the terms in the output photon flux Φ_o given in (16.3-10) that depend on the refractive index of the crystal.

16.3-2 **Longitudinal Modes.** A current is injected into an InGaAsP diode of bandgap energy $E_g = 0.91$ eV and refractive index $n = 3.5$ such that the difference in Fermi levels is $E_{fc} - E_{fv} = 0.96$ eV. If the resonator is of length $d = 250$ μm and has no losses, determine the maximum number of longitudinal modes that can oscillate.

16.3-3 **Minimum Gain Required for Lasing.** A 500-μm-long InGaAsP crystal operates at a wavelength where its refractive index $n = 3.5$. Neglecting scattering and other losses, determine the gain coefficient required to barely compensate for reflection losses at the crystal boundaries.

*16.3-4 **Modal Spacings with a Wavelength-Dependent Refractive Index.** The frequency separation of the modes of a laser diode is complicated by the fact that the refractive index is wavelength dependent [i.e., $n = n(\lambda_o)$]. A laser diode of length 430 μm oscillates at a central wavelength $\lambda_c = 650$ nm. Within the emission

bandwidth, $n(\lambda_o)$ may be assumed to be linearly dependent on λ_o [i.e., $n(\lambda_o) = n_0 - a(\lambda_o - \lambda_c)$, where $n_0 = n(\lambda_c) = 3.4$ and $a = dn/d\lambda_o$].

(a) The separation between the laser modes with wavelength near λ_c was observed to be $\Delta\lambda \approx 0.12$ nm. Explain why this does not correspond to the usual modal spacing $\nu_F = c/2d$.

(b) Find an estimate of a.

(c) Explain the phenomenon of mode pulling in a gas laser and compare it with the effect described above in semiconductor lasers.